

















## ARTICLE

# Large pH oscillations promote host defense against human airways infection

Dusik Kim<sup>1,2</sup> , Jie Liao<sup>1,2</sup> , Nathan B. Scales<sup>1,2</sup> , Carolina Martini<sup>1,2</sup> , Xiaojie Luan<sup>3</sup> , Asmahan Abu-Arish<sup>1,2</sup> , Renaud Robert<sup>1,2</sup> , Yishan Luo<sup>1,2</sup> , Geoffrey A. McKay<sup>4</sup> , Dao Nguyen<sup>2,4</sup> , Marc A. Tewfik<sup>2,4,5</sup> , Charles D. Poirier<sup>6</sup> , Elias Matouk<sup>2,7</sup> , Juan P. Iwanowski<sup>3</sup> , Saul Frenkel<sup>2,4,5</sup> , and John W. Hanrahan<sup>1,2,4</sup> 

**The airway mucosal microenvironment is crucial for host defense against inhaled pathogens but remains poorly understood. We report here that the airway surface normally undergoes surprisingly large excursions in pH during breathing that can reach pH 9.0 during inhalation, making it the most alkaline fluid in the body. Transient alkalization requires luminal bicarbonate and membrane-bound carbonic anhydrase 12 (CA12) and is antimicrobial. Luminal bicarbonate concentration and CA12 expression are both reduced in cystic fibrosis (CF), and mucus accumulation both buffers the pH and obstructs airflow, further suppressing the oscillations and bacterial-killing efficacy. Defective pH oscillations may compromise airway host defense in other respiratory diseases and explain CF-like airway infections in people with CA12 mutations.**

## Introduction

A microscopic film of airway surface liquid (ASL) containing water, salts, mucins, and antimicrobial factors secreted by the airway surface epithelium and submucosal glands covers the airway mucosa and serves as the first line of defense against inhaled pathogens. The airway mucosa is a unique microenvironment that experiences large (>140-fold) variations in CO<sub>2</sub> every few seconds due to tidal breathing. Normally, CO<sub>2</sub> in the airway lumen is ~5.6% during expiration of alveolar air and falls to 0.035% when room air is inspired. ASL is an open pH buffer system with an enormous surface area-to-volume ratio in which CO<sub>2</sub> can diffuse rapidly in its thin aqueous layer (Thomas and Adams, 1965). The half-time for CO<sub>2</sub> equilibration in thin aqueous films comparable to ASL is <219 ms (Uchida et al., 1983; Wu et al., 1998).

To investigate the mucosal microenvironment and its role in host defense, we began by directly measuring pH on human nasal mucosae in vivo using ultrafine capillary electrodes. Nasal epithelium has long served as a surrogate for distal airways in cystic fibrosis (CF) research, and nasal potential difference remains the most accepted in vivo assay for airway epithelial ion transport in this disease (Knowles et al., 1981). Recently, it has been shown that CF drugs have similar effects on nasal potential difference in vivo and in nasal epithelial cell cultures and that

cells from nasal and bronchial brushings respond similarly to CF drugs and are predictive of clinical efficacy (Pranke et al., 2017). Most people with CF (~95%) have chronic rhinosinusitis or polyposis, and their nasal and bronchial microbiomes are highly correlated, suggesting the bronchi may be colonized by bacteria that migrate from the paranasal sinuses (Hansen et al., 2012). Thus, despite some differences in cell composition, the nasal surface provides a useful model of lower airway ion transport and microbiology (Brewington et al., 2018). In this study, we confirmed the results obtained on nasal mucosae using well-differentiated primary cultures of human bronchial epithelial (HBE) cells.

## Results

### Breathing causes large oscillations in ASL pH

Flexible, double-barreled capillary electrodes were used to measure nasal pH (O'Donnell, 1992). One capillary contained H<sup>+</sup>-selective liquid ion exchange resin while the other contained 3 M KCl in agar and served as a reference (Fig. 1 A). The electrode tip had a minimum width of 150 μm and a maximum width of 550 μm, both of which exceed ASL height. However, the polypropylene surface of the capillaries created a meniscus

<sup>1</sup>Department of Physiology, McGill University, Montréal, Québec, Canada; <sup>2</sup>Cystic Fibrosis Translational Research Center, McGill University, Montréal, Québec, Canada; <sup>3</sup>Department of Anatomy, Physiology and Pharmacology, College of Medicine, University of Saskatchewan, Saskatoon, Saskatchewan, Canada; <sup>4</sup>Department of Medicine, McGill University, Research Institute–McGill University Health Centre, Montréal, Québec, Canada; <sup>5</sup>Department of Otolaryngology–Head and Neck Surgery, McGill University Health Centre, Montréal, Québec, Canada; <sup>6</sup>Centre Hospitalier de l'Université de Montréal, Montréal, Québec, Canada; <sup>7</sup>Adult Cystic Fibrosis Clinic, Montreal Chest Institute, McGill University Health Centre, Montréal, Québec, Canada.

Correspondence to John W. Hanrahan: [john.hanrahan@mcgill.ca](mailto:john.hanrahan@mcgill.ca).

© 2021 Kim et al. This article is distributed under the terms of an Attribution–Noncommercial–Share Alike–No Mirror Sites license for the first six months after the publication date (see <http://www.rupress.org/terms/>). After six months it is available under a Creative Commons License (Attribution–Noncommercial–Share Alike 4.0 International license, as described at <https://creativecommons.org/licenses/by-nc-sa/4.0/>).

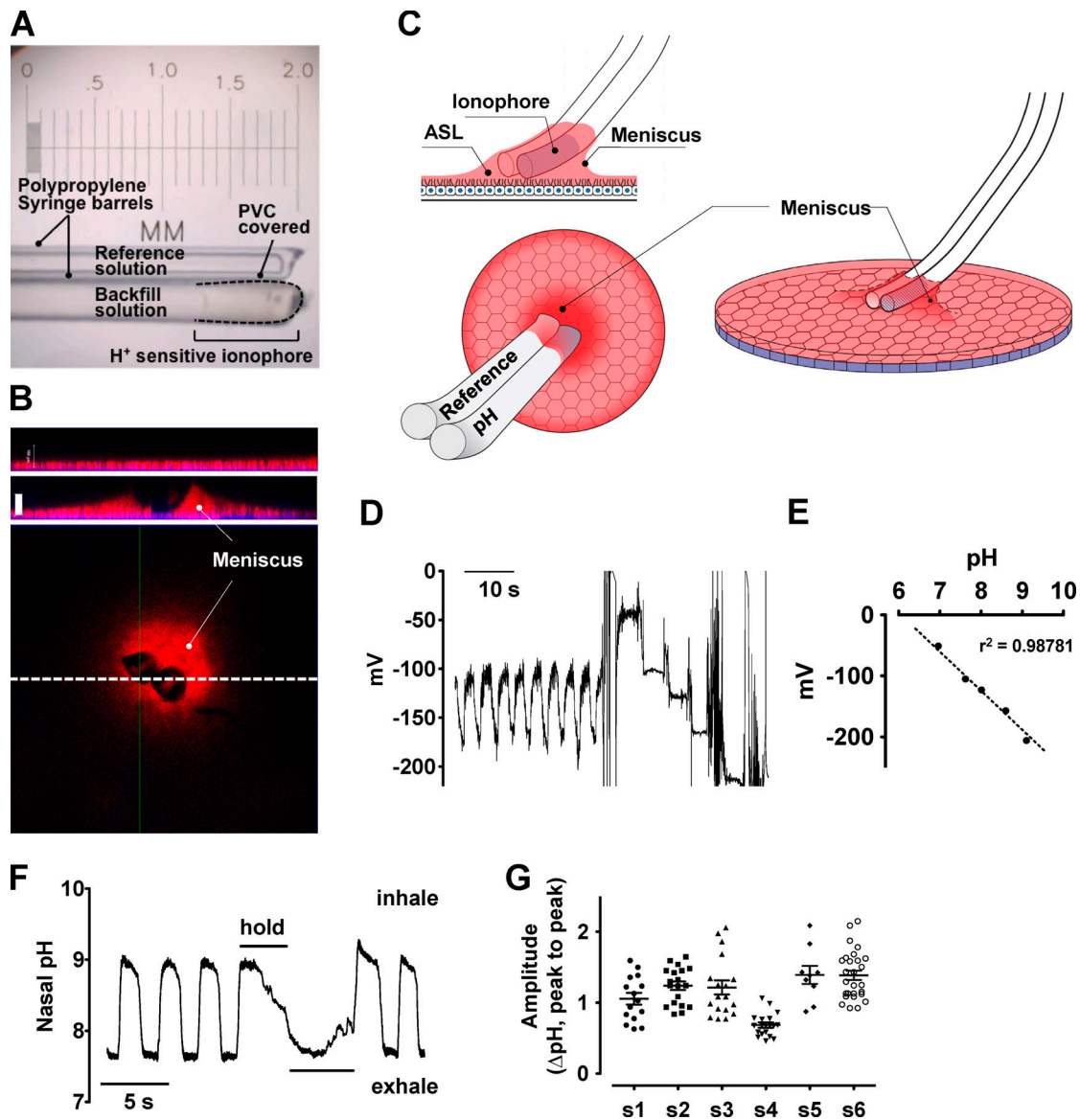


**Figure 1. Nasal pH oscillations in vivo.** (A) Double-barreled H<sup>+</sup>-selective capillary electrode. (B) Upper and middle confocal images show x-z views of artificial ASL before and after positioning electrode in artificial ASL, respectively. Bottom image shows the x-y view of same electrode tip. ASL was visualized using SNARF (SemiNaphthoRhodaFluor)-dextran (red) and cell nuclei using DAPI (blue). Vertical white scale bar = 100 μm in middle image. Red area shows ASL meniscus. Dashed line in x-y section shows location of x-z section. These images are representative of five experiments. (C) Cartoon showing electrode orientation. (D) Representative voltage recording from the nasal mucosa of a non-CF subject during breathing followed immediately by calibration in buffers with pH values (from top to bottom) 6.96, 7.62, 8.01, 8.60, and 9.10. (E) Calibration curve for the electrode shown in D. (F) Typical pH recording during tidal breathing and breath holding. (G) Summary of pH oscillation amplitude (peak to peak) on nasal mucosae of healthy subjects (s1–s6, four male and two female subjects). The error bars represent mean ± SE.

that immersed both capillaries when they were placed on bronchial cell cultures (Fig. 1, B and C). ASL height may be further increased in vivo due to mechanically induced secretion by submucosal glands. Although we could not observe the meniscus while recording in vivo, electrical continuity during nasal pH recordings confirmed that both barrels were in contact with the ASL. A new electrode was used for each subject and was calibrated in a series of buffer solutions before being placed on the inferior nasal turbinate of a healthy volunteer under visual control. We recorded the electrical potential difference between the pH-sensitive and reference barrels continuously using a

high-impedance differential amplifier while subjects took 5–10 slow breaths. Breathing caused oscillations in the voltage that had amplitudes >75 mV (Fig. 1 D). Electrodes were returned to the calibrating solutions immediately after each recording (e.g., Fig. 1 D) to confirm the electrode response and correlate measured voltages with pH (Fig. 1 E). A typical pH recording is shown in Fig. 1 F. The pH on nasal mucosae of healthy subjects oscillated between ~7.5 during exhalation and pH 8.5–9.0 during inhalation and declined during breath holding, presumably due to an accumulation of CO<sub>2</sub> (Fig. 1, F and G). The mean amplitude of excursions in pH (peak to peak) in six healthy subjects ranged

between 0.7 and 1.4 pH units (s1–s6; Fig. 1 E). These results confirm that CO<sub>2</sub> in the airway lumen equilibrates rapidly with ASL and that CO<sub>2</sub> hydration–dehydration reactions are sufficiently rapid to generate large pH changes during the breathing cycle.

### Bicarbonate and mucus modulate airway surface pH

To study ASL pH *in vitro*, we used well-differentiated primary HBE cells, which had spontaneously beating cilia and mucus-secreting goblet cells (Fulcher et al., 2005; Kim et al., 2019). We washed the cultures with PBS containing 5 mM *N*-acetylcysteine to remove accumulated mucus, then coated the cells with a thin (~10 μm) layer of artificial ASL containing both the fluorescent indicator 2',7'-bis-(2-carboxyethyl)-5-(and-6)-carboxyfluorescein (BCECF)-dextran to monitor ASL pH and the lipid soluble red styryl dye FM 1–43 to visualize the epithelium (Fig. 2 A). A computer-controlled gas-mixing pump (Fig. S1) delivered a time-varying, humidified CO<sub>2</sub>/air mixture onto the cells with a waveform resembling that in the trachea during tidal breathing (Cochrane et al., 1982). The oscillation frequency was reduced from ~0.2 to 0.017 Hz to ensure CO<sub>2</sub> mixing and efficient washout from the perfusion chamber, which was verified by comparing CO<sub>2</sub> levels at the gas inlet and exit of the chamber (Fig. 2 B, solid black and dashed red lines, respectively). CO<sub>2</sub> oscillations produced reciprocal pH changes in the artificial ASL despite weak buffering by 5 mM Hepes (Fig. 2 C). Basal pH during exposure to 5% CO<sub>2</sub> (to simulate breath exhalation) and peak pH during exposure to room air (to simulate inhalation) were both shifted to more alkaline values when the HCO<sub>3</sub><sup>-</sup> concentration was increased from 3.2 mM (Fig. 2 C, red trace) to 10 mM (Fig. 2 C, blue trace), concentrations estimated based on the pH of CF and normal airway gland secretions, respectively (Song et al., 2006). Measurements calculated from BCECF-dextran fluorescence were confirmed using a macroscopic pH electrode (Fig. 2 D).

Mucus secreted onto the airways is removed by mucociliary transport *in vivo* but accumulates over the course of several weeks when cells are cultured at the air–liquid interface. This endogenous mucus reduced the amplitude of pH oscillations (Fig. 2 E) and the rate of alkalization after a step decrease in PCO<sub>2</sub> relative to cultures that had been washed with PBS containing 5 mM *N*-acetylcysteine (Fig. 2 F). Since mucins buffer the pH of airway epithelial secretions (Kim et al., 2014), we examined the effect on the oscillations of adding exogenous mucins at concentrations expected in non-CF and CF airways (2.5% and 8% solids, respectively; Hill et al., 2014; Martens et al., 2011). Crude mucin preparations (80% pure) were used, as the properties of highly purified mucins can differ from those of native mucus and because we were interested in physiological effects on pH rather than properties of the mucins. When cultures were washed and covered with a small volume of artificial ASL sufficient to produce a layer ~10 μm high (verified using image z-stacks obtained with a confocal microscope), the pH oscillation amplitude decreased to ~1.1 pH units with 2.5% mucins (25 mg/ml) and was decreased another 40% by the addition of 8% mucins (80 mg/ml; Fig. 2 G). These results with exogenously added crude mucins resemble those obtained when

mucus secreted by the cells accumulated on the cultures (compare Fig. 2 E). In both instances, mucin buffering had little effect during exposure to 5% CO<sub>2</sub>, with pH remaining near 7. By contrast, the maximum pH during air exposure was progressively reduced, and the rate of alkalization after a step decrease in PCO<sub>2</sub> from 5% to 0.035% was slowed (Fig. 2 H). Strong buffering in the oscillating pH range was confirmed by microtitration, which indicated a buffer capacity β = 60 mM/pH with 8% solids (Fig. 2 I; gray indicates oscillatory pH range) in agreement with previous studies (Kim et al., 2014).

### Membrane-tethered carbonic anhydrase is required for mucosal pH oscillations

Computer simulations predict that large pH oscillations can occur only if CO<sub>2</sub> hydration and dehydration reactions (CO<sub>2</sub> + H<sub>2</sub>O ⇌ H<sup>+</sup> + HCO<sub>3</sub><sup>-</sup>) are rapid compared with the breathing cycle, and this would require catalysis by carbonic anhydrase (Fig. 2, J and K). ASL does not contain soluble carbonic anhydrase (Candiano et al., 2007; Thornell et al., 2018), and we observed large pH oscillations when artificial ASL lacking this enzyme was placed on washed bronchial cultures; therefore, we hypothesized that carbonic anhydrase activity is associated with the epithelial surface. As a test, we added the broad-spectrum carbonic anhydrase inhibitor acetazolamide (100 μM) or topiramate (200 μM), an inhibitor that is moderately selective for carbonic anhydrase 12 (CA12), to the artificial ASL on washed cultures and measured the rate at which pH increased after stepping PCO<sub>2</sub> from 5% to 0.035% (Fig. 2 L). Both carbonic anhydrase inhibitors reduced the rate of alkalization >50% compared with controls, indicating carbonic anhydrase activity on the apical surface of HBE cells (Fig. 2 M). Also shown for comparison are the alkalization rates when mucus had accumulated (without wash) and after addition of exogenous carbonic anhydrase type 2 (1 unit/ml; Sigma-Aldrich). To examine the effect of mucus and the role of carbonic anhydrase *in vivo*, we sprayed nasal mucosae of non-CF subjects with sterile control saline (Fig. 3, A and B) or saline containing sterilized crude mucins (8%; Fig. 3, C and D) or 500 μM acetazolamide (Fig. 3, E and F). Mucins and the carbonic anhydrase inhibitor both reduced the amplitude of breathing-induced pH excursions by >50% (Fig. 3 G).

Four of the 14 human carbonic anhydrase isozymes are membrane associated (CA4, CA9, CA12, and CA14) and could potentially catalyze changes in ASL pH. We compared their transcript levels (normalized to GAPDH) in well-differentiated primary HBE cells from five non-CF donors using quantitative PCR (qPCR). CA12 was the most abundant enzyme (Fig. 4, A and B). We also compared CA12 mRNA levels in freshly isolated bronchial epithelial cells obtained by brushing, well-differentiated HBE cultures, and human embryonic kidney (HEK) cells expressing endogenous CA12 (as a positive control). CA12 levels were approximately twofold higher in freshly isolated cells compared with cultured cells and higher in non-CF HBE cells compared with CF HBE cells.

These results contrast with a previous report using piglet proximal large airways, which concluded that surface liquid pH would not change during breathing (Thornell et al., 2018). In an

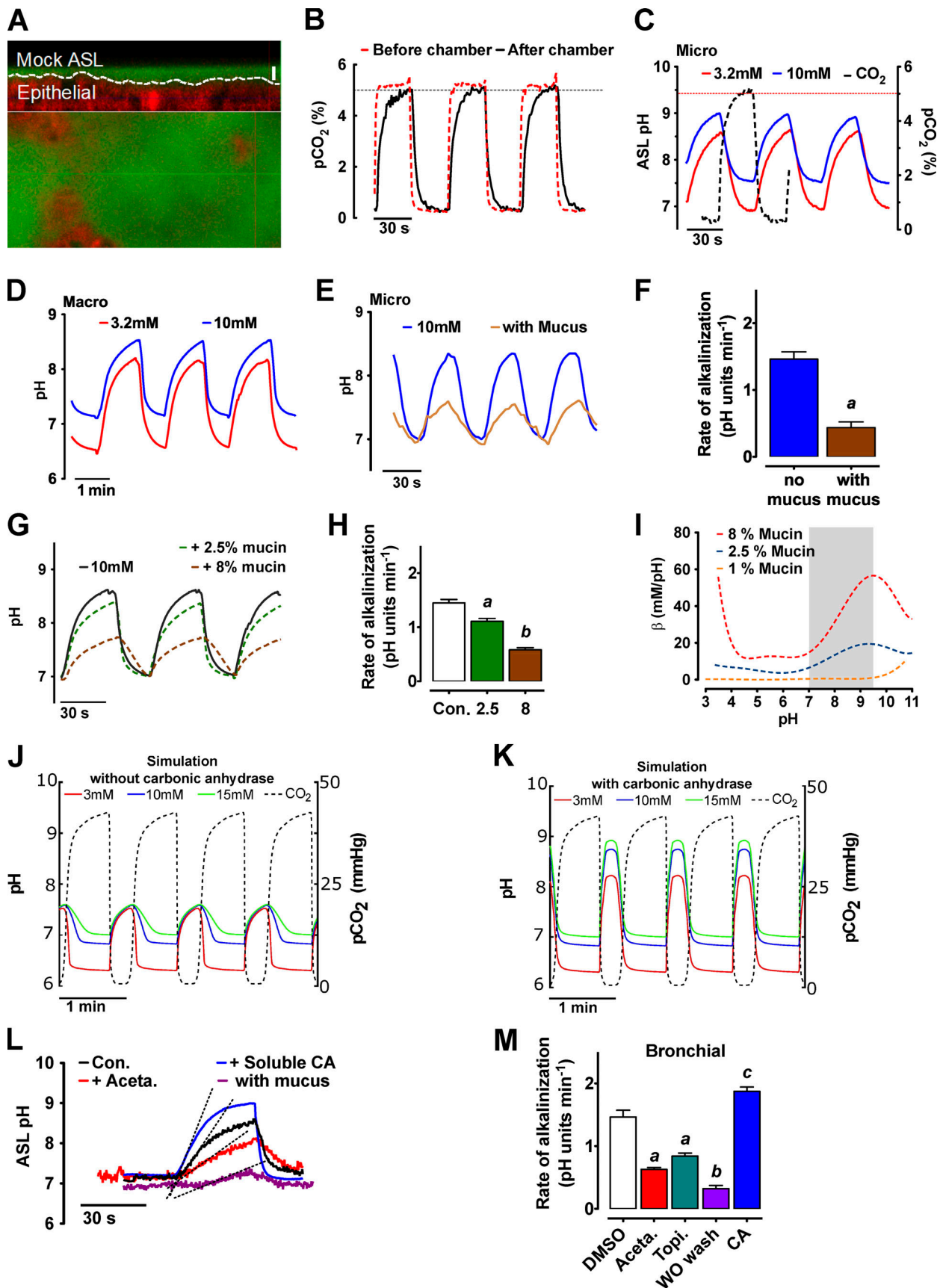


Figure 2. Large pH oscillations on cell cultures are catalyzed by membrane-bound carbonic anhydrase. (A) Confocal image of cells stained with FM-red and covered with 30  $\mu$ l artificial ASL containing pH indicator BCECF-dextran. Scale bar = 10  $\mu$ m. (B) Level of CO<sub>2</sub> at the inlet (red) and outlet (black) of the cell



chamber showing washout kinetics. **(C)** pH oscillations induced by variable  $\text{PCO}_2$  (dashed line) when artificial ASL contains 3.2 mM (red) or 10 mM (blue)  $\text{HCO}_3^-$ , measured using BCECF-dextran. **(D)** pH during  $\text{PCO}_2$  oscillations measured using a conventional microelectrode (Orion) in 100 ml artificial ASL that was bubbled vigorously using an airstone. **(E)** pH oscillations when mucus is removed (blue) or not removed (brown). **(F)** Rate of alkalinization after a step decrease in  $\text{PCO}_2$  (5%  $\rightarrow$  0.035%) when mucous secretions are removed by washing (no mucus) and when they remain (with mucus). Mean  $\pm$  SE,  $t$  test;  $n/P$  value:  $a$  (6/0.000007). **(G)** Exogenous mucus blunts oscillations when ASL containing 10 mM  $\text{HCO}_3^-$  is exposed to varying  $\text{PCO}_2$ . **(H)** Rate of alkalinization after step decrease in  $\text{PCO}_2$  (5%  $\rightarrow$  0.035%) with ASL containing 2.5% or 8% mucin solids. Mean  $\pm$  SE,  $t$  test;  $n/P$  value:  $a$  (6/0.0021) and  $b$  (6/0.0000041). **(I)** Buffer capacity (mM/pH) of mucins in the range of physiological pH oscillations (gray region). **(J)** Simulations show that pH oscillations do not reach full amplitude in the absence of carbonic anhydrase (CA) despite slow  $\text{PCO}_2$  oscillations (dashed line). **(K)** Same as J but with carbonic anhydrase. **(L)** Alkalinization rates after step decrease in  $\text{PCO}_2$  on control bronchial culture (Con.), with carbonic anhydrase inhibitor acetazolamide (Aceta., red), with exogenous soluble carbonic anhydrase (blue), or without washing off accumulated mucus (purple). **(M)** Summary of alkalinization rates on bronchial epithelial cells obtained as in L. Mean  $\pm$  SE, one-way ANOVA with post-hoc Tukey's test.  $a$ ,  $b$ , and  $c$  differences are significant;  $P = 1.8 \times 10^{-12}$  ( $n = 6-8$ ). Topi., topiramate; WO wash, without washing; CA, carbonic anhydrase.

attempt to reconcile our results, we compared CA12 mRNA transcript levels in human and pig airways. qPCR revealed extremely low CA12 mRNA expression in fresh pig tracheal scrapings and well-differentiated pig tracheal epithelial (PTE) primary cultures compared with CF bronchial tissue, well-differentiated non-CF and CF HBE cell cultures, and HEK cells expressing endogenous CA12 (Fig. 4 B). Different primers were used to amplify human and pig CA12; therefore, we also analyzed pig skeletal muscle tissue and kidney cortex as negative and positive controls. CA12 mRNA expression was negligible in pig muscle and very high in pig renal cortex, as expected. Similar results were obtained at the protein level using immunoblots (Fig. 4, C and D). Strong CA12 protein expression was observed in freshly isolated human bronchus but was also abundant in primary cultures of non-CF and CF HBE cells and in HEK cells expressing endogenous CA12. CA12 protein was expressed at high levels in pig kidney cortex, as expected, confirming that the antibody recognizes pig CA12. By contrast, CA12 protein expression was negligible in pig trachea, PTE primary cultures, and pig skeletal muscle (Fig. 4, C and D), consistent with the mRNA data in Fig. 4 B and with previous studies (Lee et al., 2016; Tarun et al., 2003). Fig. 4 D also shows very high CA12 protein expression in HEK cells that had been transiently transfected with CA12 cDNA as a positive control. These results indicate there is much higher epithelial CA12 expression in human airways than in pig airways, and this species difference may explain the previous conclusion regarding the effect of breathing on ASL pH.

Airway epithelial cells are heterogeneous; therefore, it was of interest to examine which cell types express CA12. CA12 immunofluorescence was detected at the apical pole of ciliated cells, which were readily identified by coimmunostaining with antibody against acetyl-tubulin (Fig. 4, E and F; and Fig. S2). CA12 was not detected in MUC5AC-positive goblet cells, either in well-differentiated HBE primary cultures (Fig. S2) or in tissue sections (Fig. S3 B). CA12 immunofluorescence was weaker in primary cell cultures than in freshly isolated cells obtained by nasal or bronchoscopic brushing (Fig. S4, A and B) and was also less intense in CF primary HBE cultures compared with non-CF cultures when imaged using the same microscope settings (Fig. S4, C and D), consistent with the qPCR and immunoblotting results shown in Fig. 4, B–D. The reasons for these differences in CA12 expression level remain to be elucidated and may involve such environmental and hormonal factors as oxygen tension and

estrogen receptor activation (Grubberger et al., 2001; Ivanov et al., 2001). In summary, CA12 is highly expressed in human but not pig airway epithelium. It is expressed at the apical pole of ciliated HBE cells and has an extracellular catalytic domain; thus, it may catalyze oscillations in ASL pH (Fig. 4 G).

#### Airway pH oscillations are diminished in CF

We compared breathing-induced pH changes on the nasal mucosae of 10 non-CF and seven CF subjects. During inspiration, ASL reached pH 9.0 in non-CF subjects (Fig. 5, A and C) but only pH 7.7 in those with CF (Fig. 5, B and C). pH during expiration was also 0.5 pH unit lower in CF subjects compared with non-CF subjects (Fig. 5 D). This shift to a lower baseline pH may reflect reduced ASL  $\text{HCO}_3^-$  concentration, since spraying the nasal turbinate with 50 mM sodium bicarbonate in saline increased the baseline pH by  $>0.5$  pH unit and enabled large pH excursions during breathing (compare Fig. 5, E and F, with Fig. 5, G and H). Applying  $\text{HCO}_3^-$  onto the mucosal surface increased the maximum pH during exhalation by  $>1$  pH unit. The increase was significant ( $P = 0.0051$  paired  $t$  test with four CF patients,  $P = 0.0017$  using pooled results from all CF patients; Fig. 5, I–K), indicating that exogenous  $\text{HCO}_3^-$  can restore large, breathing-induced alkalinizations of the ASL on CF nasal mucosa.

#### pH oscillations are inherently antimicrobial

The gram-negative bacterium *Pseudomonas aeruginosa* is the most common lung pathogen in CF adults and is considered a neutrophile because its growth is optimal in the range pH 6.6–7.0 (Booth, 1985; Todar, 2019). We examined the pH sensitivity of *P. aeruginosa* using the mucoid strain PA508 from a CF patient. Bacteria were incubated for 24 h in artificial ASL at pH values ranging from 7.4 to 9.1. Aliquots were then plated on agar to determine the number of viable bacteria (colony-forming units [CFUs]; Fig. 6 A). There was little killing in the range of pH 7.4–8.0, as expected; however, CFUs declined at more alkaline pH values. The time course of the decline in air-equilibrated saline suggested that  $>50\%$  of the CFUs are killed within  $\sim 3$  h under these conditions (Fig. 6 B).

We also examined the antimicrobial effect of  $\text{CO}_2$  oscillations in fluid secreted by the airway epithelial cell line Calu-3. The number of CFUs was unchanged after bacteria were incubated for 6 h in fluid from unstimulated Calu-3 airway epithelial cells that had been equilibrated with air. However, when incubated in fluid from Calu-3 cultures that had been stimulated with

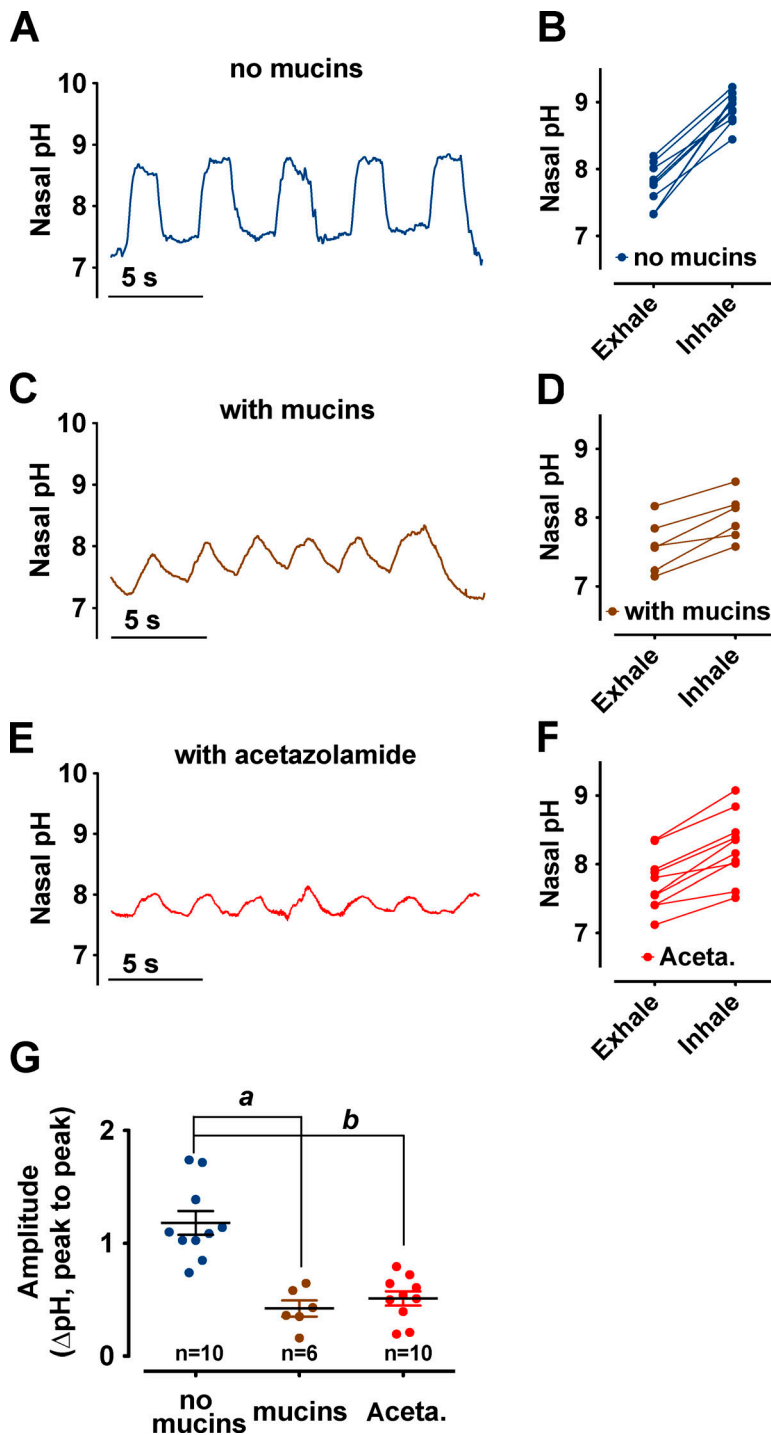


**Figure 3. Mucus buffers and carbonic anhydrase inhibitors diminish pH oscillations in vivo.** (A) Nasal pH of healthy nonsmoker volunteers was measured with capillary ion-selective electrodes. The inferior turbinate on each side was lightly sprayed with saline solution, and pH was measured after ~1 min. (B) pH differences during expiration and inspiration (each point is mean of three measurements, 10 subjects). (C and D) Effect of exogenous sterile crude mucins (8 mg/ml) on pH oscillations. (E and F) pH excursions blunted after application of carbonic anhydrase inhibitor acetazolamide (500  $\mu$ M). (G) Summary of the oscillation amplitudes showing effect of mucus and carbonic anhydrase inhibition on pH excursions. Mean  $\pm$  SE t test, compared with control ( $n = 10$  subjects);  $n/P$  value: differences a (6/0.00016) and b (10/0.000036). Aceta., acetazolamide.

forskolin (FSK) to secrete  $\text{HCO}_3^-$ -rich fluid, 90% killing was observed (Fig. 6 C, i). By contrast, the number of CFUs increased exponentially regardless of FSK stimulation when bacteria were incubated in Calu-3 secretions that had been equilibrated with 5%  $\text{CO}_2$  (Fig. 6 C, ii). Thus, elevating  $\text{PCO}_2$  in the physiological range to prevent ASL alkalization inhibits bacterial killing, and the increase in CFUs suggests that glycoproteins and other macromolecules in the secretions are nutrients that support bacterial growth. The secretions were bacteriostatic when  $\text{CO}_2$  was maintained constant at 2.5% (i.e., there was no bacterial

growth; Fig. 6 C, iii). However,  $\text{PCO}_2$  oscillations that yielded the same time-averaged  $\text{PCO}_2$  (i.e., 2.5%) were strongly antimicrobial (Fig. 6 C, iv), indicating that fluctuations in pH are inherently antimicrobial (Fig. 6 D). Similar results were obtained with artificial ASL containing a range of  $\text{HCO}_3^-$  concentrations (3.2–50 mM; Fig. 6 E). At each  $\text{HCO}_3^-$  concentration, more killing was observed when  $\text{PCO}_2$  oscillated than when it remained constant at the same mean value (i.e., 2.5%). Further evidence that the antimicrobial effect is due to pH rather than  $\text{HCO}_3^-$  was obtained using a bioluminescence assay. Increasing pH to 8.6 or

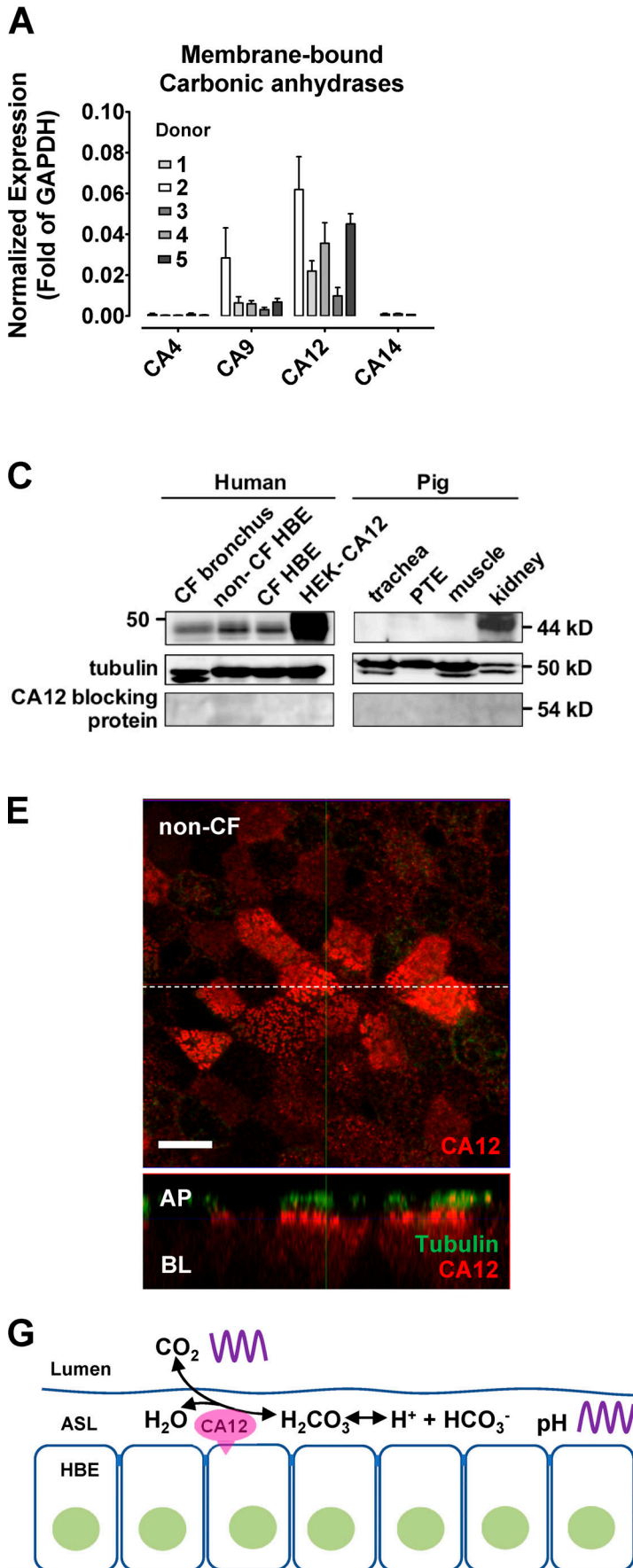


**Figure 4. Expression of membrane-associated carbonic anhydrases CA4, CA9, CA12, and CA14 in human and pig airway epithelia. (A)** mRNA levels in primary human bronchial cells ( $n = 9\text{--}12$  measurements from  $\geq 3$  cultures). Error bars represent SE. **(B)** CA12 mRNA levels normalized to GAPDH. Human: freshly isolated HBE cells, cultured non-CF and CF HBEs, and HEK cells (with endogenous CA12 expression as positive control). Pig: freshly isolated trachea, cultured PTE cells, skeletal muscle (negative control), and kidney cortex (positive control). Mean  $\pm$  SE  $t$  test, compared with pig trachea;  $n/P$  value:  $a$  (4/0.0048),  $b$  (4/0.016), and  $c$  (4/0.0778). **(C)** Immunoblot showing CA12 protein expression with tubulin as loading control. Fresh tissues were flash frozen in liquid  $N_2$ , pulverized, and extracted into lysis buffer. HEK cells were transfected with CA12 as positive control (HEK-CA12). Immunostaining was lost when antibody was preincubated with CA12 as a blocking protein. **(D)** Summary of relative levels of human and pig CA12 protein. Band densities were normalized to tubulin, and the normalized values were plotted relative to that for pig. Mean  $\pm$  SE  $t$  test, compared with pig trachea;  $n/P$  value: differences  $a$  (5/0.0036),  $b$  (5/0.0022), and  $c$  (4/0.0159). **(E)** Upper image: x-y view of HBE cells showing CA12 (red) at the apical pole (non-CF donor). Lower image: x-z view showing the apical localization of CA12 and acetylated tubulin in ciliated cells. White scale bar = 10  $\mu$ m. AP, apical; BL, basolateral. **(F)** Localization of CA12 (red) and tubulin or MUC5AC (green) in isolated, well-differentiated HBE cells from non-CF donor. White scale bar = 10  $\mu$ m. **(G)** Cartoon showing reversible hydration of  $CO_2$  in the ASL catalyzed by membrane-bound CA12.

9.3 caused similar killing in solutions buffered with phosphate or a mixture of phosphate and  $HCO_3^-$  (Fig. 6 F). Taken together, the results indicate that breathing-induced oscillations in  $PCO_2$  produce large, transient alkalinizations that are antimicrobial in both artificial ASL and epithelial secretions.

## Discussion

Rapid, oscillating changes in ASL pH are an important feature of the airway microenvironment that has not been reported previously and has broad implications for airway physiology and host defense mechanisms. It is distinct from the current paradigm in which there is a slight reduction in steady-state pH in CF airways (Pezzulo et al., 2012). pH measurements using antimony and gold pH probes have not detected a lower steady-state pH in CF compared with non-CF subjects (McShane et al., 2003), and bronchial pH was not altered in CF versus non-CF children when measured using a luminescent dye-based fiber-optic probe having dimensions similar to the capillary electrodes used here (Schultz et al., 2017). Although we observed a slightly lower baseline pH on CF nasal epithelium in vivo, a more striking finding was the presence of large excursions to high pH during breathing that were absent or greatly reduced in CF subjects.

Previous modeling suggested that ASL pH oscillations would not occur during breathing due to low carbonic anhydrase activity (Thornell et al., 2018); however, the conclusion was based on data from pig airways. We found that airway CA12 expression is up to 100-fold higher in humans, and this species difference may account for different conclusions in the previous study. CA12 is a type I membrane protein with an extracellular catalytic domain and is expressed on the apical surface of many epithelia (Lee et al., 2016). Its physiological role remains uncertain in most tissues; however, in salivary glands it is essential for  $HCO_3^-$  secretion (Hong et al., 2015). In the renal proximal tubule, membrane-bound carbonic anhydrases CA4 and CA14 facilitate  $HCO_3^-$  reabsorption by accelerating its conversion to  $CO_2$  in the lumen (Purkerson and Schwartz, 2007). The present results suggest that in the airways, membrane-bound CA12 accelerates  $CO_2$  hydration and dehydration reactions so that they approach equilibrium during the breathing cycle, generating large pH oscillations.

Several factors are expected to influence the amplitude of pH oscillations. They require luminal  $HCO_3^-$ , which is reduced in CF (Smith and Welsh, 1992) due to diminished CF transmembrane

conductance regulator (CFTR)-mediated  $HCO_3^-$  efflux (Linsdell et al., 1997; Poulsen et al., 1994) and also reduced  $HCO_3^-$  secretion by pendrin (SLC26A4), an anion exchanger that is modulated by CFTR (Gorrieri et al., 2016; Kim et al., 2019). The steady-state  $HCO_3^-$  concentration in ASL will also be reduced by concurrent  $H^+$  secretion via mechanisms that continue unabated when CFTR-dependent  $HCO_3^-$  secretion is defective (Coakley et al., 2003; Li et al., 2016; Scudieri et al., 2018). Abnormal mucus is a hallmark of CF (Quinton, 2008), and we found that buffering by endogenous mucous secretions and exogenous, semi-purified mucins reduces the pH excursions. Mucus accumulation and airway obstruction would reduce the amplitude of pH excursions further, since airflow is required for variations in  $PCO_2$ . Loss of alkaline transients may impact other respiratory diseases in which there is excess mucus and *Pseudomonas* infection, such as chronic obstructive pulmonary disease and non-CF bronchiectasis.

We found that a constant, low level of  $CO_2$  is less antimicrobial than  $PCO_2$  oscillations that have the same mean  $PCO_2$  value. This may reflect greater cell stress when bacteria must maintain intracellular pH homeostasis in a fluctuating environment. In addition to direct bacterial killing, excursions to high pH in vivo may exert antimicrobial effects through other mechanisms, for example, by increasing the efficacy of cationic antimicrobial peptides (Abou Alaiwa et al., 2014) or through enhanced oxidative killing by the dual oxidase-lactoperoxidase system (Iovannisci et al., 2010). HBE mucus properties vary little in the range of pH 6.0–8 (Hill et al., 2018); however, the present results encourage studies of rheological properties and mucus plugging at higher pH (Tang et al., 2016). We observed similar pH oscillations on the nasal mucosae of male and female subjects and on cultured cells from male and female subjects; however, future studies should also examine sex differences systematically, as CF females acquire *P. aeruginosa* infections earlier in life (Demko et al., 1995) and have more frequent pulmonary exacerbations (Block et al., 2006). Estrogen may suppress pH oscillations by inhibiting  $HCO_3^-$  secretion (Sheridan et al., 2013) or by reducing the sensitivity of bacteria to pH by inducing mucoidy (i.e., bacterial secretion of a protective, alginate-containing matrix; Chotirmall et al., 2012).

Using alkalinization when air is inhaled to kill pathogens contained in that air requires rapid  $CO_2$  hydration and dehydration reactions catalyzed by carbonic anhydrase. This may explain why mutations in CA12 produce lung disease with



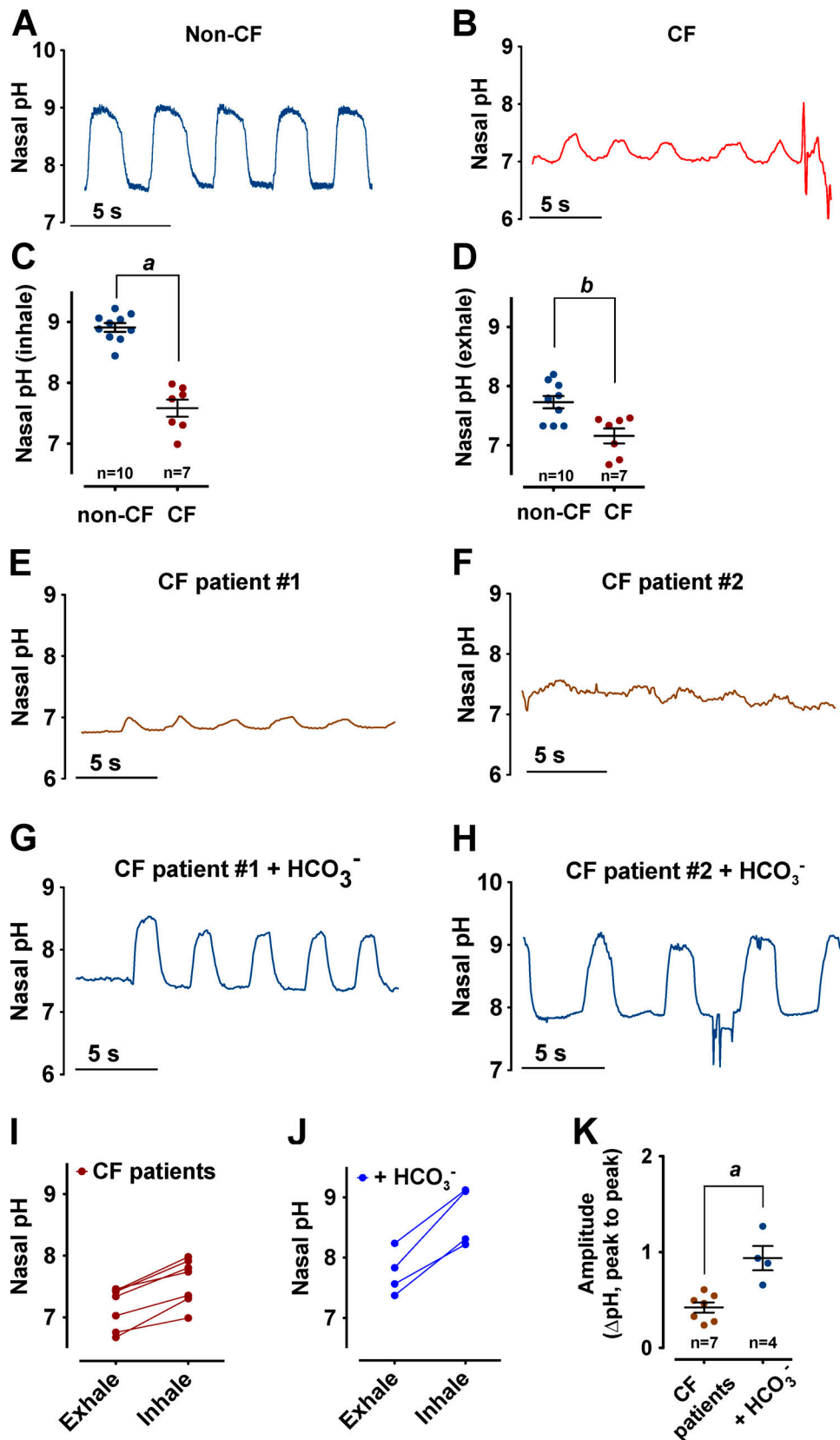


Figure 5. **Excursions of pH are reduced in CF.** (A and B) Recordings from non-CF (A) and CF (B) nasal mucosae showing more acidic basal pH and smaller alkalinizations during inhalation in CF subject with genotype 3876delA/1811+1643G>T. (C and D) Summary of nasal pH during inhalation and exhalation in non-CF and CF subjects. Mean ± SE, *t* test, *n* = 10; *n*/P value: difference *a* (P = 7/1.6 × 10<sup>-7</sup>) and difference *b* (P = 7/0.0032). (E and F) Recordings of nasal pH during tidal breathing in CF subjects with genotypes G542X/711+1G>T (#1) and 2789+G>A/2347delG (#2), respectively. (G and H) Nasal pH during breathing in the

same subjects as in E and F after nasal mucosa was lightly sprayed with 50 mM bicarbonate solution. **(I and J)** Surface pH on CF nasal epithelia during exhalation and inhalation when sprayed with saline lacking (I) or containing (J)  $\text{HCO}_3^-$ , respectively. Subject genotypes: F508/W1282X, 3876delA/1811+1643G>T, G542X/711+1G>T, 1677delTA/1677delTA, 2789+5G>A/2347delG, F508/3272-26A>G, F508del/F508del (tested without  $\text{HCO}_3^-$ ); 1677delTA/1677delTA, G542X/711+1G>T, 3876delA/1811+1643G>T, and F508del/F508del (tested with  $\text{HCO}_3^-$ ). **(K)** Oscillation amplitudes on CF nasal surface sprayed with saline or 50 mM  $\text{HCO}_3^-$  solution. Mean  $\pm$  SE, t test, comparison to control ( $n = 7$ );  $n/P$  value: difference  $a$  (4/0.0017).

symptoms resembling those in CF (Lee et al., 2016). An American adult misdiagnosed with CF and a boy from a consanguineous Bedouin family who displayed classic CF symptoms without mutations in the *cftr* gene were both found to be homozygous for loss-of-function mutations in CA12. It would be interesting to measure ASL pH in these individuals to determine if an inability to alkalize ASL pH during inhalation might explain their susceptibility to respiratory infections.

## Materials and methods

### Subjects and primary cultures

In vivo measurements of pH on the nasal mucosa were performed with informed written consent following protocol #MM-CODIM-16-296, which was approved by the West-Central-Montreal-Health's Medical/Biomedical Research Ethics Committee. Nasal pH was measured in 10 adult control subjects: mean age, 30.8 yr (range, 24–38 yr); six males. Nasal pH was also measured in 11 subjects with CF carrying a range of CF mutations: mean age was 30.2 yr (range, 22–47 yr); eight subjects were males, and all genotypes are indicated in the figure legends.

For in vitro studies of pH on nasal and bronchial epithelial cell cultures, non-CF lung tissue was obtained from the International Institute for the Advancement of Medicine (Edison, NJ) and National Disease Research Interchange (Philadelphia, PA). CF bronchial tissue from patients undergoing lung transplantation was obtained with informed written consent from the Biobank of respiratory tissues at the Centre Hospitalier de l'Université de Montréal and Institut de recherche cliniques de Montréal. Tissue handling followed protocols approved by the institutional review boards of the Centre Hospitalier de l'Université de Montréal and McGill University (#A08-M70-14B). HBE cells were isolated in the Primary Airway Cell Biobank at the McGill Cystic Fibrosis Translational Research center as described previously (Fulcher et al., 2005; Matthes et al., 2018) and cultured for 1 mo under an air-liquid interface. All CF cells used for in vitro studies were homozygous for F508del-CFTR.

### Nasal ASL pH measured in vivo using flexible ion-selective capillary electrodes

Electrodes ~1 m in length were constructed by heating and pulling 1-ml disposable polyethylene syringes (Becton Dickinson) into fine capillaries (O'Donnell, 1992). An internal reference solution (mM: 100 NaCl and 100 sodium citrate, pH 6) was injected into the back of the syringe. The tip was filled by capillarity with a 1–2-mm column of hydrogen ionophore I-cocktail B (Sigma-Aldrich) and coated with 15% (wt/vol) polyvinyl chloride in tetrahydrofuran to prevent leakage of the ion exchanger. A silver chloride wire was inserted into the internal

reference solution and connected by a cable to a differential electrometer (HiZ-223; Warner Instruments) interfaced to a computer (PowerLab 2/26; AD Instruments). The reference electrode was filled with 3 M KCl in 3% agar, and the two flexible capillaries were glued together using 15% PVC (polyvinyl chloride). Capillary pH electrodes had response times <1 s. The voltage was digitized, displayed, and stored on a personal computer. The double-barreled ion-selective electrodes were calibrated in phosphate-buffered solutions adjusted to pH 6.5–9.5 before and immediately after recording nasal pH. The mean  $\pm$  SE for slopes and  $r^2$  values were  $-51.1 \pm 3.0$  mV and  $0.9851 \pm 0.0027$ , respectively, for  $n = 32$  electrodes.

A new capillary electrode was used for each subject and was placed gently on the inferior nasal turbinate. Subjects were asked to hold their breath for 10 s, then take 5–10 slow breaths while pH was being recorded. Recordings were annotated to indicate inhalation and exhalation. In some experiments, the turbinate was lightly sprayed with solution containing 50 mM bicarbonate, 500  $\mu\text{M}$  acetazolamide, or filter-sterilized pig gastric mucins (80 mg/ml). pH recordings were analyzed using LabChart 7 (AD Instruments). Statistics were performed using Prism 5 software (GraphPad).

### Bronchial ASL pH measured in vitro using fluorescence imaging

Air-liquid interface cultures contained columnar cells with beating cilia and goblet cells with mucin granules. Mucus accumulated on the apical surface and was removed before most experiments by rinsing with PBS containing 5 mM *N*-acetylcysteine. Bronchial epithelial cultures were mounted in a closed chamber during  $\text{CO}_2$  oscillations on the stage of an inverted fluorescence microscope (IX81; Olympus) equipped with an imaging system (Photon Technology International) as described (Kim et al., 2019). Cells were rinsed with artificial ASL (mM: 130 NaCl, 10  $\text{NaHCO}_3$ , 5 KCl, 1  $\text{CaCl}_2$ , 1  $\text{MgSO}_4$ , 2.8 NaHepes, 2.2 Hepes acid, and 10 glucose) and covered with 30  $\mu\text{l}$  artificial ASL for at least 30 min before measurements. The ratiometric fluorescent pH indicator BCECF conjugated to dextran (Molecular Probes; Thermo Fisher Scientific) was added to artificial ASL using the vehicle FC-72, a perfluorocarbon that evaporated rapidly from the surface. To mimic tidal breathing, cells were exposed to alternating flows of 0.035% and 5%  $\text{CO}_2$  using a custom-designed gas-mixing pump equipped with a humidification system and interfaced to a computer (Okolab).  $\text{CO}_2$  levels at the gas inlet and outlet ports of the perfusion chamber were measured using an infrared  $\text{CO}_2$  analyzer (CD-3A; Applied Biosystem). In some experiments, purified carbonic anhydrase type 2 (1 unit; Sigma-Aldrich) or the carbonic anhydrase inhibitor acetazolamide (100  $\mu\text{M}$ ) or topiramate

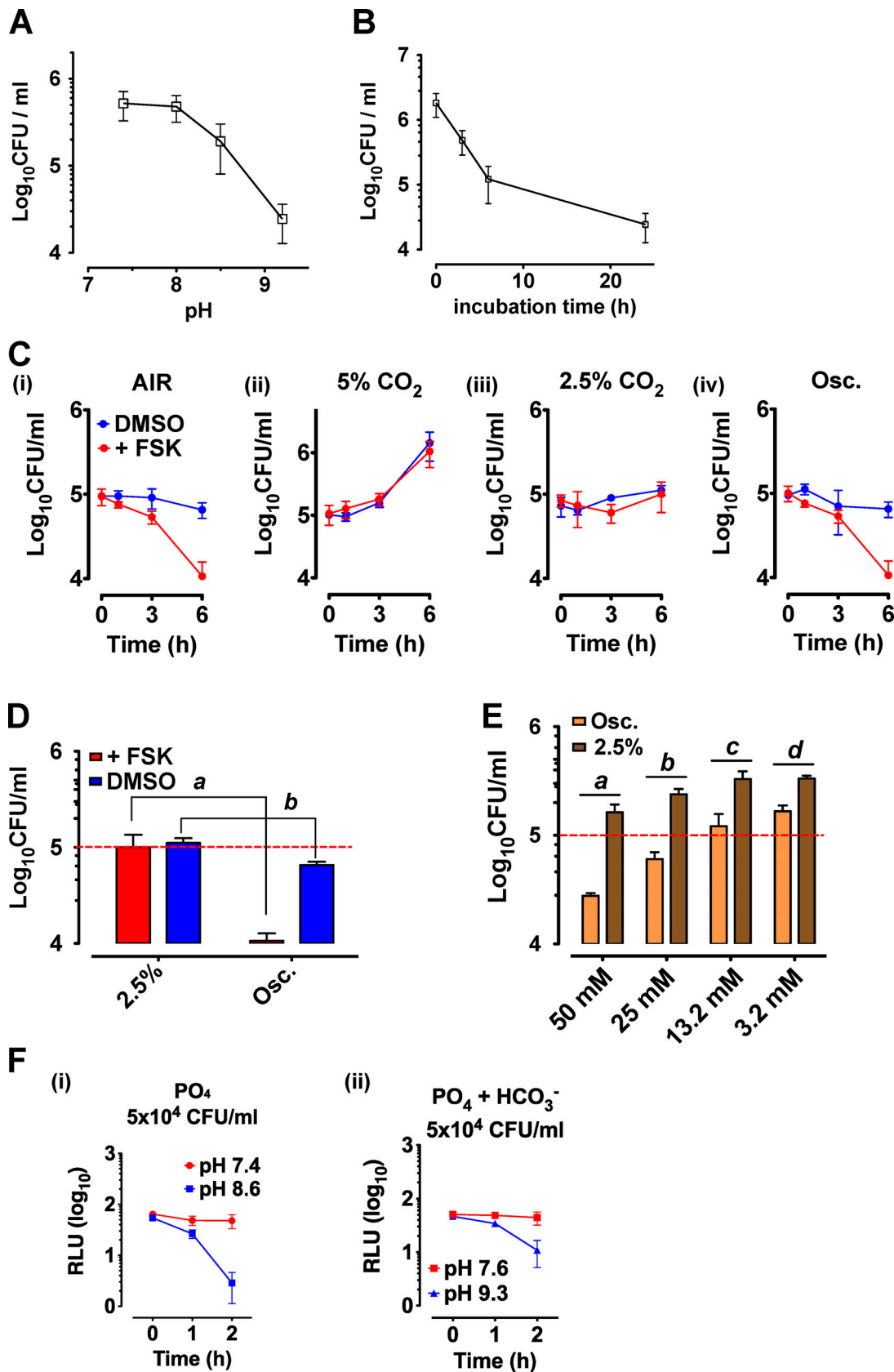


Figure 6. **Oscillations enhance bacterial killing at high pH.** (A) pH dependence of *Pseudomonas* killing after 24-h exposure to air-equilibrated artificial ASL (mM: 115 NaCl, 1.2 CaCl<sub>2</sub>, 1.2 MgCl<sub>2</sub>, and 25 NaHCO<sub>3</sub>) plus 100 mM NaHPO<sub>4</sub>/Na<sub>2</sub>PO<sub>4</sub> with ratio adjusted to give indicated pH. Mean ± SD, n = 3. (B) Time course of killing in air-equilibrated artificial ASL (pH -9.2, mean ± SD, n = 3). (C) Antimicrobial effects of airway epithelial secretions. Bacteria were incubated for 6 h in

fluid secreted by Calu-3 cells treated with DMSO (vehicle control) or FSK (10  $\mu\text{M}$ ) to stimulate bicarbonate secretion. **(i)** No proliferation when equilibrated with air (0.035%  $\text{CO}_2$ ). Viable bacteria (CFUs) were unchanged in control secretions (blue) and reduced 10-fold in stimulated secretions (red). **(ii)** Proliferation in constant 5%  $\text{CO}_2$ . **(iii)** No proliferation or killing in constant 2.5%  $\text{CO}_2$ . **(iv)** Oscillations with median  $\text{PCO}_2 \approx 2.5\%$  prevented growth in control secretions but caused killing in stimulated secretions. **(D)** Comparison of antimicrobial effect of secretions when equilibrated with constant 2.5%  $\text{CO}_2$  or with  $\text{CO}_2$  oscillations with mean  $\text{CO}_2 = 2.5\%$ . Dashed red line shows initial CFUs. Oscillations increase sensitivity to alkaline pH. Mean  $\pm$  SE, *t* test, compared with 2.5%  $\text{PCO}_2$  ( $n = 6$ ); *n/P* value: difference *a* (6/0.0207) and difference *b* (6/0.0079). **(E)** Antimicrobial effect of  $\text{PCO}_2$  oscillations in artificial ASL (mM: 115 NaCl, 1.2  $\text{CaCl}_2$ , 1.2  $\text{MgCl}_2$ , and varying concentrations of  $\text{NaHCO}_3$  from 3.2 to 50 mM). Mean  $\pm$  SE, *t* test comparing constant  $\text{PCO}_2$  versus oscillations ( $n = 4$ ); *n/P* value: differences *a* (4/0.0121), *b* (4/0.0035), *c* (4/0.0367), and *d* (4/0.0026). **(F)** Antimicrobial effect of 2-h exposure to 100 mM  $\text{NaH}_2\text{PO}_4/\text{Na}_2\text{PO}_4$  solution without  $\text{HCO}_3^-$  adjusted to pH 7.4 (red) or 8.6 (blue; *i*); *ii* same as *i* but with 10  $\text{NaHCO}_3$  added and pH 7.6 and 9.3. Error bars in C and F represent SE. RLU, relative luminescence units.

(200  $\mu\text{M}$ ) was added to the artificial ASL. The effects of mucins on pH oscillations were studied by adding porcine gastric mucins (20–80 mg/ml; Sigma-Aldrich) dissolved in artificial ASL.

### Immunoblotting

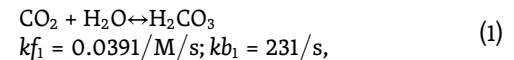
Well-polarized primary cultures were scraped from Transwells and solubilized in RIPA lysis buffer (150 mmol/L NaCl, 1 mmol/L Tris/HCl, 1% deoxycholic acid, 1% Triton X-100, 0.1% SDS, and protease inhibitor) for 15–30 min at 22°C and centrifuged at 32,000 *g* for 15 min at 22°C. Pig tissues (trachea, skeletal muscle, and kidney cortex) were snap frozen in liquid nitrogen immediately after dissection and stored at  $-80^\circ\text{C}$  for up to 2 wk, ground into a fine powder using mortar and pestle, then solubilized in RIPA buffer. HEK cells expressing endogenous CA12 or transfected with CA12 cDNA were used as positive controls in immunoblots. Cells at 50%–80% confluence were transfected in 100-mm Petri dishes with 4  $\mu\text{g}$  CA12 cDNA (OriGene) using GeneJuice (Sigma-Aldrich) as per manufacturer's instructions. Supernatants were collected and assayed for protein concentration (Bio-Rad). Samples containing 50  $\mu\text{g}$  total protein were resolved using 10% SDS-PAGE and transferred to nitrocellulose membranes. Membranes were blocked with 5% skimmed milk in TBST (20 mM Tris-HCl, pH 7.4, 150 mM NaCl, 1% Tween 20) for 1 h at 22°C, then incubated with anti-CA12 (1:500; Proteintech) and anti-tubulin (clone KMX-1; 1:1,000; Millipore Sigma) overnight at 4°C. Cross-reactivity of the anti-CA12 antibody with the pig enzyme was established using skeletal muscle and renal cortex as negative and positive controls, respectively. Cross-reactivity of the anti-tubulin antibody with pig tubulin was confirmed by immunostaining cilia in pig trachea. The membranes were washed with TBST, and the bands were visualized using Amersham Bioscience ECL (enhanced chemiluminescence) detecting reagent (GE Healthcare) and a ChemiDoc Imaging System (Bio-Rad).

### Computer simulations

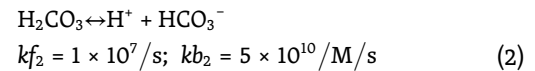
To predict airway surface pH during  $\text{CO}_2$  oscillations, numerical simulations were performed using Matlab (The Mathworks). We assumed physiological dimensions for ASL thickness, *L*, so that diffusion effects would be negligible within the breathing period, *T*, which is justified since the effects of diffusion can be neglected when the ratio of the breathing period to the diffusion time is relatively large ( $DT/L^2 > 1$ ), a condition that is satisfied for *L* < 65  $\mu\text{m}$  and a period of 4 s for one breath. This enabled us

to model bicarbonate-buffered ASL using a system of ordinary differential equations (ODEs).

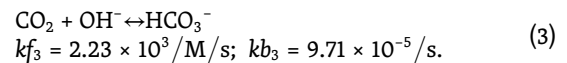
$\text{CO}_2$  in the ASL combines with water to form carbonic acid according to the (uncatalyzed) reaction



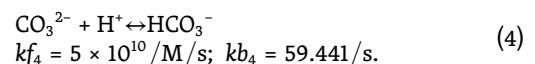
where  $k_{f1}$  and  $k_{b1}$  are the forward and reverse rate constants, respectively. The following reactions and rate constants were used to model the dissociation of carbonic acid into bicarbonate and the reaction of  $\text{CO}_2$  with the hydroxyl ions (Eq. 2, Mitchell et al., 2010; Eq. 3, Schulz et al., 2006):



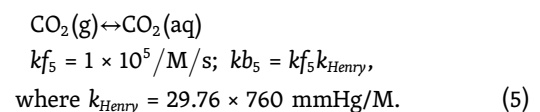
and



It was assumed that epithelial cells maintain bicarbonate concentration in the ASL at 3 mM and 10 mM in CF and non-CF ASL, respectively. Competition for the  $\text{H}^+$  ion by the reaction of carbonate with  $\text{H}^+$  to form bicarbonate was added to reproduce the slow overall rate expected for the uncatalyzed system (Eq. 4, Schulz et al., 2006):



At the airway surface, gaseous  $\text{CO}_2$  was kept in equilibrium with the aqueous  $\text{CO}_2$  in the ASL using Mitchell et al. (2010):



The concentration of  $\text{OH}^-$  was calculated at each time step by assuming charge balance (i.e., the net positive charge must equal the net negative charge). Charge balance requires

$$\text{H}^+ = \text{OH}^- + \text{HCO}_3^- + 2\text{CO}_3^{2-}, \quad (6)$$

which can be rearranged to solve for the hydroxide concentration:

$$\text{OH}^- = \text{H}^+ - \text{HCO}_3^- - 2\text{CO}_3^{2-}. \quad (7)$$

The above reactions were converted into the following system of ODEs:



$$\left. \begin{aligned}
 d[\text{CO}_2(\text{g})]/dt &= -kf_5[\text{CO}_2(\text{g})] + kb_5[\text{CO}_2(\text{aq})] \\
 d[\text{CO}_2(\text{aq})]/dt &= -kf_1[\text{CO}_2(\text{aq})] + kb_1[\text{H}_2\text{CO}_3] \\
 &\quad + kf_5[\text{CO}_2(\text{g})] - kb_5[\text{CO}_2(\text{aq})] - \\
 &\quad kf_3[\text{CO}_2(\text{aq})][\text{OH}^-] + kb_3[\text{HCO}_3^-] \\
 d[\text{H}_2\text{CO}_3]/dt &= kf_1[\text{CO}_2(\text{aq})] - kb_1[\text{H}_2\text{CO}_3] - \\
 &\quad kf_2[\text{H}_2\text{CO}_3] + kb_2[\text{H}^+][\text{HCO}_3^-] \\
 d[\text{HCO}_3^-]/dt &= kf_2[\text{H}_2\text{CO}_3] - kb_2[\text{H}^+][\text{HCO}_3^-] + \\
 &\quad kf_3[\text{CO}_2(\text{aq})][\text{OH}^-] - kb_3[\text{HCO}_3^-] + \\
 &\quad kf_4[\text{CO}_3^{2-}][\text{H}^+] - kb_4[\text{HCO}_3^-] \\
 d[\text{H}^+]/dt &= kf_2[\text{H}_2\text{CO}_3] - kb_2[\text{H}^+][\text{HCO}_3^-] - \\
 &\quad kf_4[\text{CO}_3^{2-}][\text{H}^+] - kb_4[\text{HCO}_3^-] \\
 d[\text{CO}_3^{2-}]/dt &= -kf_4[\text{CO}_3^{2-}][\text{H}^+] + kb_4[\text{HCO}_3^-]
 \end{aligned} \right\} \quad (8)$$

Initial conditions for the system were set to

$$\left. \begin{aligned}
 [\text{CO}_2(\text{g})](t=0) &= \text{input oscillatory CO}_2(\text{g}) \text{ waveform} \\
 [\text{CO}_2(\text{aq})](t=0) &= [\text{CO}_2(\text{g})](t=0)(29.76 \times 760) \\
 [\text{H}_2\text{CO}_3](t=0) &= 0.1 \mu\text{M} \\
 [\text{HCO}_3^-](t=0) &= [\text{HCO}_3^-] \text{ input} \\
 [\text{H}^+](t=0) &= 0.1 \mu\text{M} \\
 [\text{CO}_3^{2-}](t=0) &= 0.1 \text{ nM}
 \end{aligned} \right\} \quad (9)$$

The input  $\text{CO}_2$  waveform was generated by digitizing a published  $\text{CO}_2$  recording (Cochrane et al., 1982), extracting a single breath from the digitized waveform, and then smoothing it. This single breath was then scaled in amplitude and time as needed to generate a series of breaths.

This system of ODEs can be considered very stiff and was solved using ode15s with a very low absolute and relative tolerance ( $10^{-18}$  and  $10^{-15}$ , respectively) using the NonNegative option. To simulate the presence of carbonic anhydrase, the above system was modified by increasing  $kb_1$  and  $kf_1$  by a factor of 20,000. We modified  $kb_2$  in Eq. 2 to be  $2.14 \times 10^{10}/\text{M/s}$  to better match the pH values predicted by the Henderson-Hasselbalch equation for the bicarbonate buffer system. This modification yields a theoretical  $\text{pK}_a$  of 6.1 for the system defined by Eqs. 1 and 2, rather than 6.47 using the rate of  $5 \times 10^{10}/\text{M/s}$  used by Mitchell et al. (2010).

### Real-time qPCR

First-strand cDNA was prepared using 1  $\mu\text{g}$  total RNA and SuperScript VILO MasterMix (Invitrogen). CA12 mRNA levels were determined using Taqman primers (Assay ID: CA12: Hs01080909\_m1; Life Technologies). Reactions were analyzed using the Quant Studio 7 Flex Real-Time PCR system (Life Technologies) and “Fast” program:  $95^\circ\text{C}$  for 20 s, followed by 40 cycles of  $95^\circ\text{C}$  for 1 s and  $60^\circ\text{C}$  for 20 s. Data were normalized to GAPDH mRNA levels.

### Immunostaining bronchial sections and primary cultures

Tissue specimens were collected within 48 h of lung resection and fixed in 10% neutral buffered formalin at  $4^\circ\text{C}$  overnight for paraffin embedding and sectioning. Tissue sections (5  $\mu\text{m}$ ) were mounted on microscope slides, de-paraffinized in xylene ( $3 \times 5$  min), and rehydrated in alcohol baths (95%, 95%, 70%; 5 min each) followed by two 5-min rinses in double-distilled  $\text{H}_2\text{O}$  and equilibration in PBS. Sections were permeabilized using 1% Triton X-100 and blocked for 1 h with 2% BSA in PBS at room temperature, then incubated with primary antibody (rabbit anti-CA12 1:200; Proteintech Group Inc.; mouse anti-Tubulin 1:

200; MilliporeSigma; or mouse anti-MUC5AC 1:200; MilliporeSigma) in 1% BSA/PBS for 1 h. They were then exposed to Alexa-488 goat anti-mouse and Alexa-594 goat anti-rabbit secondary antibody (1:200; Abcam) for 1 h and mounted in ProLong Diamond Antifade Mountant (Invitrogen). Immunofluorescence was imaged using an LSM-780 confocal microscope (Zeiss) with a multiline Argon laser (488 nm, 25 mW) and a 561-nm line laser (15 mW). For primary cells on filters, the apical side was incubated with PBS for 15 min at  $37^\circ\text{C}$  in 5%  $\text{CO}_2$ , rinsed three times to remove apical mucus, and immunostained as above. To image single cells, air-liquid interface cultures were washed with PBS at room temperature, gently scraped from the inserts into PBS, then centrifuged onto a glass slide using a Cytospin4 (500 rpm for 5 min; Thermo Fisher Scientific).

### Antimicrobial activity

CFU assays of viable bacteria used the mucoid strain *P. aeruginosa* 508 kindly provided by Dr. Danuta Radzioch (Research Institute-McGill University Health Centre, Montréal, Canada). *P. aeruginosa* suspensions were prepared using fresh colonies from tryptic soy broth (TSB) agar plates as follows: bacteria were cultured overnight in 50 ml TSB (250 rpm,  $37^\circ\text{C}$ ), then cultured in fresh TSB for 2–3 h until mid-log phase growth as determined by optical density at 600 nm. Bacteria were washed in sterile PBS (pH 7.2, 10 mM) and diluted to  $10^5$ – $10^6$  cells/ml in epithelial secretions or artificial ASL with slight modifications as detailed in the legends for Fig. 6 and Fig. S5. Secretions were used immediately after collection from Calu-3 cells that had been cultured at an air-liquid interface for at least 10 d. Apical fluid was collected by pipette under control conditions or during stimulation with 10  $\mu\text{M}$  FSK. TSB (1%) was added to artificial ASL as a nutrient source in some experiments (Fig. 6 E and Fig. S5). For the killing assays in Fig. 6, A, B, and F, bacteria and test fluids were placed in small polypropylene chambers with loose-fitting caps and incubated for up to 24 h. In the experiments shown in Fig. 6, C–E, a chamber was connected to the computer-controlled  $\text{CO}_2$  gas-mixing pump shown in Fig. S1, and 500- $\mu\text{l}$  aliquots containing bacteria were exposed to constant or oscillating  $\text{PCO}_2$  for up to 6 h in a humidified incubator at  $37^\circ\text{C}$ . Bacteria were sampled from the chambers as indicated in Fig. 6 and plated in duplicate on agar plates. After incubating the plates overnight at  $37^\circ\text{C}$ , CFUs were counted using OpenCFU software (Geissmann, 2013).

Bioluminescence assays of bacterial killing used the PAO1-DN613 strain of *P. aeruginosa* in which the *rpsL*-lux reporter was integrated into the chromosome at the *attB* site using a pUC18-mini-Tn7T vector. Bacterial samples were prepared from fresh colonies on plates and grown to mid-logarithmic phase for 2.5 h after overnight culture. Bacteria were suspended in sterile PBS at  $10^9$  CFUs/ml, then serially diluted to  $10^2$ /ml in bicarbonate or phosphate buffer (100 mM). To calibrate the bioluminescence signal, 100- $\mu\text{l}$  aliquots of bacteria at each dilution were transferred into tubes, and their bioluminescence was measured using a luminometer (TD-20/20; Turner Designs). To assess viability under different conditions, the samples were placed in an incubator shaker at  $36^\circ\text{C}$ , incubated with orbital agitation at 200 rpm for 0, 1, and 2 h, and then vortexed briefly before measuring bioluminescence.

## Data availability

Requests for computer code should be addressed to Nathan B. Scales: nscales@gmail.com.

## Online supplemental material

**Fig. S1** shows the programmable fast gas-mixing pump, which is used to mimic variations in  $\text{PCO}_2$  during tidal breathing when measuring the surface pH on well-differentiated primary bronchial epithelial cells in vitro. **Fig. S2** shows that CA12 protein is expressed in ciliated cells but not secretory cells. **Fig. S3** shows the specificity of the CA12 antibody used for immunostaining human lung tissue. **Fig. S4** shows that CA12 immunostaining is reduced in CF bronchial and nasal cell cultures compared with non-CF cell cultures. **Fig. S5** shows that  $\text{HCO}_3^-$ -dependent killing is enhanced by  $\text{PCO}_2$  oscillations in the presence of nutrients.

## Acknowledgments

We are grateful to the research subjects who volunteered to participate in the clinical studies. We thank Dr. Jacopo Mortola (McGill University, Montréal, Québec, Canada) for access to infrared  $\text{CO}_2$  monitoring equipment, Dr. Danuta Radzioch (Research Institute-McGill University Health Centre, Montréal, Québec, Canada) for bacterial strains, Véronique Flynn and Olymel S.E.C. (Saint-Esprit, Québec, Canada) for providing pig tissue, and Hong-Seok Hur for preparing the graphical abstract and graphic in **Fig. 1**.

This work was supported by research grants from Cystic Fibrosis Canada (grant no. 3022) and the Canada Foundation for Innovation (grant no. 21375) to J.W. Hanrahan and Cystic Fibrosis Canada (grant no. 555681) to J.P. Ianowski.

Author contributions: D. Kim, S. Frenkiel, E. Matouk, R. Robert, and J.W. Hanrahan planned the project; D. Kim, C. Martini, M.A. Tewfik, C.D. Poirier, X. Luan, G.A. McKay, D. Nguyen, and J.P. Ianowski developed the tools; N.B. Scales wrote the software and performed the computer simulations; D. Kim, J. Liao, A. Abu-Arish, Y. Luo, and S. Frenkiel performed the experiments; D. Kim, J. Liao, and N.B. Scales analyzed the data; and D. Kim and J.W. Hanrahan wrote the manuscript. All authors helped to interpret the results and reviewed and approved the manuscript.

Disclosures: M.A. Tewfik reported "other" from Sanofi, "other" from AstraZeneca, personal fees from Novartis, personal fees from Mylan, and personal fees from Stryker outside the submitted work. No other disclosures were reported.

Submitted: 26 August 2020

Revised: 1 November 2020

Accepted: 18 November 2020

## References

Abou Alaiwa, M.H., L.R. Reznikov, N.D. Gansemer, K.A. Sheets, A.R. Horswill, D.A. Stoltz, J. Zabner, and M.J. Welsh. 2014. pH modulates the activity and synergism of the airway surface liquid antimicrobials beta-defensin-3 and LL-37. *Proc. Natl. Acad. Sci. USA.* 111:18703–18708. <https://doi.org/10.1073/pnas.1422091112>

Block, J.K., K.L. Vandemheen, E. Tullis, D. Fergusson, S. Doucette, D. Haase, Y. Berthiaume, N. Brown, P. Wilcox, P. Bye, et al. 2006. Predictors of

pulmonary exacerbations in patients with cystic fibrosis infected with multi-resistant bacteria. *Thorax.* 61:969–974. <https://doi.org/10.1136/thx.2006.061366>

Booth, I.R. 1985. Regulation of Cytoplasmic Ph in Bacteria. *Microbiol. Rev.* 49: 359–378. <https://doi.org/10.1128/MMBR.49.4.359-378.1985>

Brewington, J.J., E.T. Filbrandt, F.J. LaRosa III, J.D. Moncivaiz, A.J. Ostmann, L.M. Strecker, and J.P. Clancy. 2018. Brushed nasal epithelial cells are a surrogate for bronchial epithelial CFTR studies. *JCI Insight.* 3:e99385. <https://doi.org/10.1172/jci.insight.99385>

Candiano, G., M. Bruschi, N. Pedemonte, L. Musante, R. Ravazzolo, S. Liberatori, L. Bini, L.J. Galletta, and O. Zegarra-Moran. 2007. Proteomic analysis of the airway surface liquid: modulation by proinflammatory cytokines. *Am. J. Physiol. Lung Cell. Mol. Physiol.* 292:L185–L198. <https://doi.org/10.1152/ajplung.00085.2006>

Chotirmall, S.H., S.G. Smith, C. Gunaratnam, S. Cosgrove, B.D. Dimitrov, S.J. O'Neill, B.J. Harvey, C.M. Greene, and N.G. McElvaney. 2012. Effect of estrogen on pseudomonas mucoidy and exacerbations in cystic fibrosis. *N. Engl. J. Med.* 366:1978–1986. <https://doi.org/10.1056/NEJMoa1106126>

Coakley, R.D., B.R. Grubb, A.M. Paradiso, J.T. Gatzky, L.G. Johnson, S.M. Kreda, W.K. O'Neal, and R.C. Boucher. 2003. Abnormal surface liquid pH regulation by cultured cystic fibrosis bronchial epithelium. *Proc. Natl. Acad. Sci. USA.* 100:16083–16088. <https://doi.org/10.1073/pnas.2634339100>

Cochrane, C.M., C.G. Newstead, R.V. Nowell, P. Openshaw, and C.B. Wolff. 1982. The rate of rise of alveolar carbon dioxide pressure during expiration in man. *J. Physiol.* 333:17–27. <https://doi.org/10.1113/jphysiol.1982.sp014435>

Demko, C.A., P.J. Byard, and P.B. Davis. 1995. Gender differences in cystic fibrosis: Pseudomonas aeruginosa infection. *J. Clin. Epidemiol.* 48: 1041–1049. [https://doi.org/10.1016/0895-4356\(94\)00230-N](https://doi.org/10.1016/0895-4356(94)00230-N)

Fulcher, M.L., S. Gabriel, K.A. Burns, J.R. Yankaskas, and S.H. Randell. 2005. Well-differentiated human airway epithelial cell cultures. In *Human Cell Culture Protocols*. J. Picot, editor. Humana Press, Totowa, NJ. pp. 183–206.

Geissmann, Q. 2013. OpenCFU, a new free and open-source software to count cell colonies and other circular objects. *PLoS One.* 8:e54072. <https://doi.org/10.1371/journal.pone.0054072>

Gorrieri, G., P. Scudieri, E. Caci, M. Schiavon, V. Tomati, F. Sirci, F. Napolitano, D. Carrella, A. Gianotti, I. Musante, et al. 2016. Goblet Cell Hyperplasia Requires High Bicarbonate Transport To Support Mucin Release. *Sci. Rep.* 6:36016. <https://doi.org/10.1038/srep36016>

Gruvberger, S., M. Ringner, Y. Chen, S. Panavally, L.H. Saal, A. Borg, M. Ferno, C. Peterson, and P.S. Meltzer. 2001. Estrogen receptor status in breast cancer is associated with remarkably distinct gene expression patterns. *Cancer Res.* 61:5979–5984.

Hansen, S.K., M.H. Rau, H.K. Johansen, O. Ciofu, L. Jelsbak, L. Yang, A. Folkesson, H.O. Jarmer, K. Aanaes, C. von Buchwald, et al. 2012. Evolution and diversification of Pseudomonas aeruginosa in the paranasal sinuses of cystic fibrosis children have implications for chronic lung infection. *ISME J.* 6:31–45. <https://doi.org/10.1038/ismej.2011.83>

Hill, D.B., P.A. Vasquez, J. Mellnik, S.A. McKinley, A. Vose, F. Mu, A.G. Henderson, S.H. Donaldson, N.E. Alexis, R.C. Boucher, et al. 2014. A biophysical basis for mucus solids concentration as a candidate biomarker for airways disease. *PLoS One.* 9:e87681. <https://doi.org/10.1371/journal.pone.0087681>

Hill, D.B., R.F. Long, W.J. Kissner, E. Atieh, I.C. Garbarine, M.R. Markovetz, N.C. Fontana, M. Christy, M. Habibpour, R. Tarran, et al. 2018. Pathological mucus and impaired mucus clearance in cystic fibrosis patients result from increased concentration, not altered pH. *Eur. Respir. J.* 52: 1801297. <https://doi.org/10.1183/13993003.01297-2018>

Hong, J.H., E. Muhammad, C. Zheng, E. Hershkovitz, S. Alkrinawi, N. Loewenthal, R. Parvari, and S. Muallem. 2015. Essential role of carbonic anhydrase XII in secretory gland fluid and  $\text{HCO}_3^-$  secretion revealed by disease causing human mutation. *J. Physiol.* 593:5299–5312. <https://doi.org/10.1113/JP271378>

Iovannisci, D., B. Illek, and H. Fischer. 2010. Function of the HVCN1 proton channel in airway epithelia and a naturally occurring mutation, M91T. *J. Gen. Physiol.* 136:35–46. <https://doi.org/10.1085/jgp.200910379>

Ivanov, S., S.Y. Liao, A. Ivanova, A. Danilkovitch-Miagkova, N. Tarasova, G. Weirich, M.J. Merrill, M.A. Proescholdt, E.H. Oldfield, J. Lee, et al. 2001. Expression of hypoxia-inducible cell-surface transmembrane carbonic anhydrases in human cancer. *Am. J. Pathol.* 158:905–919. [https://doi.org/10.1016/S0002-9440\(10\)64038-2](https://doi.org/10.1016/S0002-9440(10)64038-2)

Kim, D., J. Liao, and J.W. Hanrahan. 2014. The buffer capacity of airway epithelial secretions. *Front. Physiol.* 5:188. <https://doi.org/10.3389/fphys.2014.00188>

- Kim, D., J. Huang, A. Billet, A. Abu-Arish, J. Goepp, E. Matthes, M.A. Tewfik, S. Frenkiel, and J.W. Hanrahan. 2019. Pendrin Mediates Bicarbonate Secretion and Enhances Cystic Fibrosis Transmembrane Conductance Regulator Function in Airway Surface Epithelia. *Am. J. Respir. Cell Mol. Biol.* 60:705–716. <https://doi.org/10.1165/rcmb.2018-0158OC>
- Knowles, M., J. Gatzky, and R. Boucher. 1981. Increased bioelectric potential difference across respiratory epithelia in cystic fibrosis. *N. Engl. J. Med.* 305:1489–1495. <https://doi.org/10.1056/NEJM198112173052502>
- Lee, M., B. Vecchio-Pagan, N. Sharma, A. Waheed, X. Li, K.S. Raraigh, S. Robbins, S.T. Han, A.L. Franca, M.J. Pellicore, et al. 2016. Loss of carbonic anhydrase XII function in individuals with elevated sweat chloride concentration and pulmonary airway disease. *Hum. Mol. Genet.* 25:1923–1933. <https://doi.org/10.1093/hmg/ddw065>
- Li, X., X.X. Tang, L.G. Vargas Buonfiglio, A.P. Comellas, I.M. Thornell, S. Ramachandran, P.H. Karp, P.J. Taft, K. Sheets, M.H. Abou Alaiwa, et al. 2016. Electrolyte transport properties in distal small airways from cystic fibrosis pigs with implications for host defense. *Am. J. Physiol. Lung Cell. Mol. Physiol.* 310:L670–L679. <https://doi.org/10.1152/ajplung.00422.2015>
- Linsdell, P., J.A. Tabcharani, J.M. Rommens, Y.-X. Hou, X.-B. Chang, L.-C. Tsui, J.R. Riordan, and J.W. Hanrahan. 1997. Permeability of wild-type and mutant cystic fibrosis transmembrane conductance regulator chloride channels to polyatomic anions. *J. Gen. Physiol.* 110:355–364. <https://doi.org/10.1085/jgp.110.4.355>
- Martens, C.J., S.K. Inglis, V.G. Valentine, J. Garrison, G.E. Conner, and S.T. Ballard. 2011. Mucous solids and liquid secretion by airways: studies with normal pig, cystic fibrosis human, and non-cystic fibrosis human bronchi. *Am. J. Physiol. Lung Cell. Mol. Physiol.* 301:L236–L246. <https://doi.org/10.1152/ajplung.00388.2010>
- Matthes, E., J. Goepp, C. Martini, J. Shan, J. Liao, D.Y. Thomas, and J.W. Hanrahan. 2018. Variable Responses to CFTR Correctors in vitro: Estimating the Design Effect in Precision Medicine. *Front. Pharmacol.* 9:1490. <https://doi.org/10.3389/fphar.2018.01490>
- McShane, D., J.C. Davies, M.G. Davies, A. Bush, D.M. Geddes, and E.W. Alton. 2003. Airway surface pH in subjects with cystic fibrosis. *Eur. Respir. J.* 21:37–42. <https://doi.org/10.1183/09031936.03.00027603>
- Mitchell, M.J., O.E. Jensen, K.A. Cliffe, and M.M. Maroto-Valer. 2010. A model of carbon dioxide dissolution and mineral carbonation kinetics. *Proc. R. Soc. A.* 466:1265–1290. <https://doi.org/10.1098/rspa.2009.0349>
- O'Donnell, M.J. 1992. A simple method for construction of flexible, miniature ion-selective electrodes. *J. Exp. Biol.* 162:353–359.
- Pezzulo, A.A., X.X. Tang, M.J. Hoegger, M.H. Alaiwa, S. Ramachandran, T.O. Moninger, P.H. Karp, C.L. Wohlford-Lenane, H.P. Haagsman, M. van Eijk, et al. 2012. Reduced airway surface pH impairs bacterial killing in the porcine cystic fibrosis lung. *Nature.* 487:109–113. <https://doi.org/10.1038/nature11130>
- Poulsen, J.H., H. Fischer, B. Illek, and T.E. Machen. 1994. Bicarbonate conductance and pH regulatory capability of cystic fibrosis transmembrane conductance regulator. *Proc. Natl. Acad. Sci. USA.* 91:5340–5344. <https://doi.org/10.1073/pnas.91.12.5340>
- Pranke, I.M., A. Hatton, J. Simonin, J.P. Jais, F. Le Pimpec-Barthes, A. Carsin, P. Bonnette, M. Fayon, N. Stremmer-Le Bel, D. Grenet, et al. 2017. Correction of CFTR function in nasal epithelial cells from cystic fibrosis patients predicts improvement of respiratory function by CFTR modulators. *Sci. Rep.* 7:7375. <https://doi.org/10.1038/s41598-017-07504-1>
- Purkerson, J.M., and G.J. Schwartz. 2007. The role of carbonic anhydrases in renal physiology. *Kidney Int.* 71:103–115. <https://doi.org/10.1038/sj.ki.5002020>
- Quinton, P.M. 2008. Cystic fibrosis: impaired bicarbonate secretion and mucoviscidosis. *Lancet.* 372:415–417. [https://doi.org/10.1016/S0140-6736\(08\)61162-9](https://doi.org/10.1016/S0140-6736(08)61162-9)
- Schultz, A., R. Puvvadi, S.M. Borisov, N.C. Shaw, I. Klimant, L.J. Berry, S.T. Montgomery, T. Nguyen, S.M. Kreda, A. Kicic, et al. 2017. Airway surface liquid pH is not acidic in children with cystic fibrosis. *Nat. Commun.* 8:1409. <https://doi.org/10.1038/s41467-017-00532-5>
- Schulz, K.G., U. Riebesell, B. Rost, S. Thoms, and R.E. Zeebe. 2006. Determination of the rate constants for the carbon dioxide to bicarbonate inter-conversion in pH-buffered seawater systems. *Mar. Chem.* 100:53–65. <https://doi.org/10.1016/j.marchem.2005.11.001>
- Scudieri, P., I. Musante, E. Caci, A. Venturini, P. Morelli, C. Walter, D. Tosi, A. Palleschi, P. Martin-Vasallo, I. Sermet-Gaudelus, et al. 2018. Increased expression of ATP12A proton pump in cystic fibrosis airways. *JCI Insight.* 3:e123616. <https://doi.org/10.1172/jci.insight.123616>
- Sheridan, J.T., R.C. Gilmore, M.J. Watson, C.B. Archer, and R. Tarran. 2013. 17beta-Estradiol inhibits phosphorylation of stromal interaction molecule 1 (STIM1) protein: implication for store-operated calcium entry and chronic lung diseases. *J. Biol. Chem.* 288:33509–33518. <https://doi.org/10.1074/jbc.M113.486662>
- Smith, J.J., and M.J. Welsh. 1992. cAMP stimulates bicarbonate secretion across normal, but not cystic fibrosis airway epithelia. *J. Clin. Invest.* 89:1148–1153. <https://doi.org/10.1172/JCI115696>
- Song, Y., D. Salinas, D.W. Nielson, and A.S. Verkman. 2006. Hyperacidity of secreted fluid from submucosal glands in early cystic fibrosis. *Am. J. Physiol. Cell Physiol.* 290:C741–C749. <https://doi.org/10.1152/ajpcell.00379.2005>
- Tang, X.X., L.S. Ostedgaard, M.J. Hoegger, T.O. Moninger, P.H. Karp, J.D. McMenimen, B. Choudhury, A. Varki, D.A. Stoltz, and M.J. Welsh. 2016. Acidic pH increases airway surface liquid viscosity in cystic fibrosis. *J. Clin. Invest.* 126:879–891. <https://doi.org/10.1172/JCI83922>
- Tarun, A.S., B. Bryant, W. Zhai, C. Solomon, and D. Shusterman. 2003. Gene expression for carbonic anhydrase isoenzymes in human nasal mucosa. *Chem. Senses.* 28:621–629. <https://doi.org/10.1093/chemse/bjg054>
- Thomas, W.J., and M.J. Adams. 1965. Measurement of the diffusion coefficients of carbon dioxide and nitrous oxide in water and aqueous solutions of glycerol. *Trans. Faraday Soc.* 61:668–673. <https://doi.org/10.1039/tf9656100668>
- Thornell, I.M., X. Li, X.X. Tang, C.M. Brommel, P.H. Karp, M.J. Welsh, and J. Zabner. 2018. Nominal carbonic anhydrase activity minimizes airway-surface liquid pH changes during breathing. *Physiol. Rep.* 6:e13569. <https://doi.org/10.14814/phy2.13569>
- Todar, K.G. 2019. *Todar's Online Textbook of Bacteriology.* <http://www.textbookofbacteriology.net> (accessed July 23, 2019).
- Uchida, K., M. Mochizuki, and K. Niizeki. 1983. Diffusion coefficients of CO<sub>2</sub> molecule and bicarbonate ion in hemoglobin solution measured by fluorescence technique. *Jpn. J. Physiol.* 33:619–634. <https://doi.org/10.2170/jjphysiol.33.619>
- Wu, D.X.-Y., C.Y.C. Lee, S.N. Uyekubo, H.K. Choi, S.J. Bastacky, and J.H. Widdicombe. 1998. Regulation of the depth of surface liquid in bovine trachea. *Am. J. Physiol. Lung Cell. Mol. Physiol.* 274:L388–L395. <https://doi.org/10.1152/ajplung.1998.274.3.L388>

Supplemental material

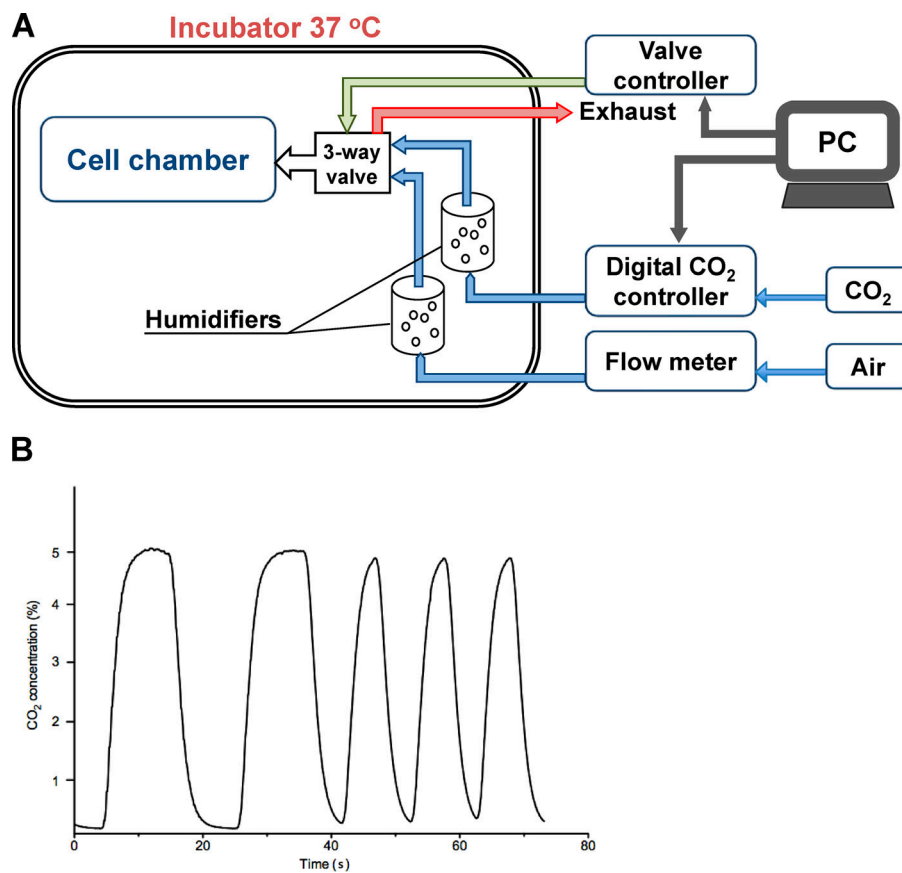


Figure S1. **Programmable fast gas-mixing pump.** (A) Schematic of computer-driven valve and CO<sub>2</sub> controllers, humidification system, and cell chamber. (B) Recording of the PCO<sub>2</sub> supplied by the gas-mixing pump, measured using an infrared CO<sub>2</sub> analyzer (CD-3A; Applied Biosystem) at oscillation frequencies of 0.05 Hz and 0.1 Hz.



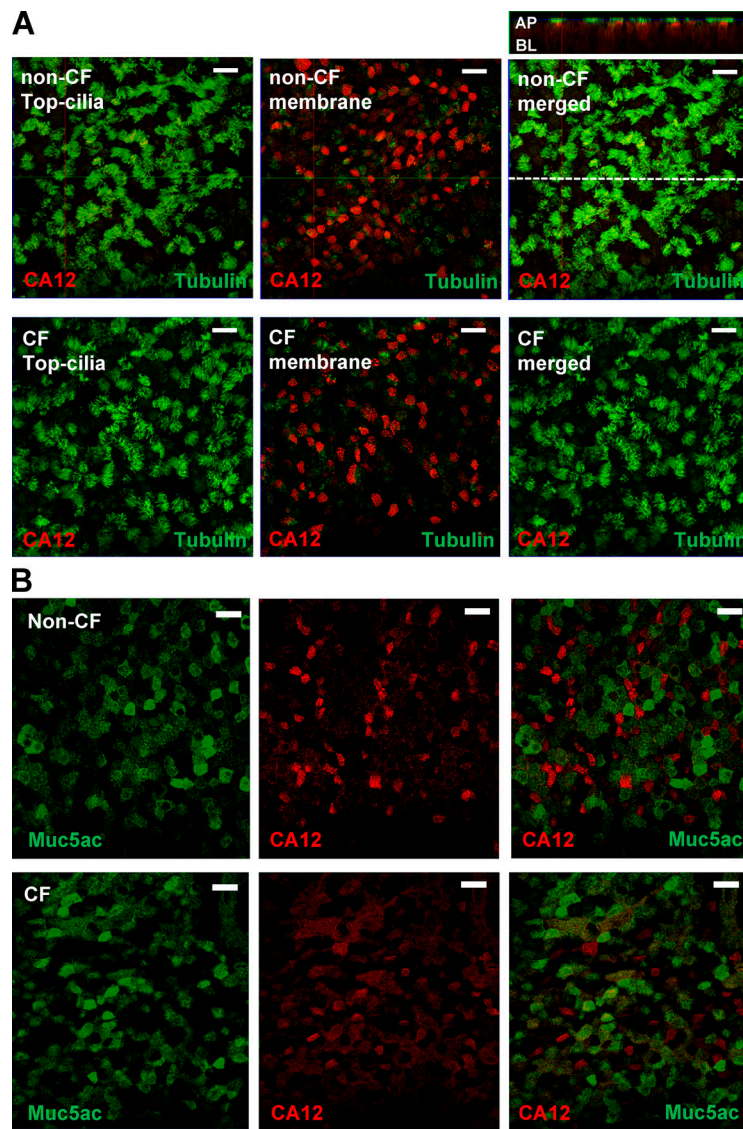


Figure S2. **CA12 is expressed in ciliated cells not goblet cells. (A)** Well-differentiated HBEs from non-CF (upper images) and CF (lower images) donors show the colocalization of CA12 with tubulin. Left images show cilia as tubulin immunofluorescence. Middle images show strong CA12 expression after re-focusing on the apical cell surface. Merging these images on the right reveals that CA12 expression is exclusively in ciliated cells. Top right image (x-z view) shows CA12 immunofluorescence immediately beneath cilia. AP, apical; BL, basolateral. Scale bars = 20  $\mu\text{m}$ . **(B)** CA12 (red) and MUC5AC (green) immunostaining of well-differentiated non-CF (upper images) and CF (lower images) HBEs. CA12 and MUC5AC immunofluorescence was not observed in the same cells. CF cultures had more goblet cells and fewer CA12-expressing cells, which may explain the reduced CA12 expression shown in Fig.4. Scale bars = 20  $\mu\text{m}$ .

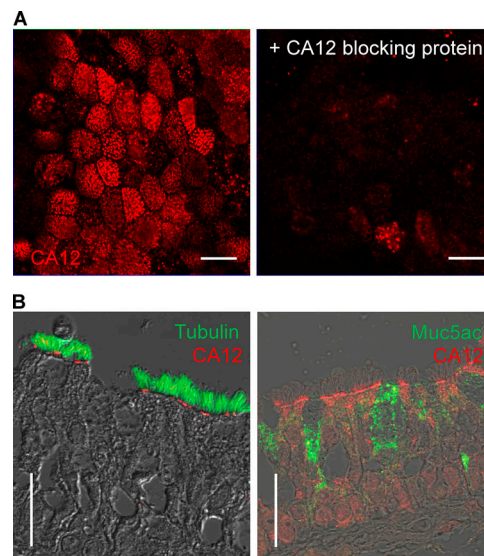


Figure S3. **CA12 antibody specificity and immunostaining in human lung tissue.** **(A)** Most CA12 immunostaining at the apical pole of ciliated cells was abolished by excess recombinant CA12 as a blocking protein. Scale bars = 10  $\mu\text{m}$ . **(B)** CA12 signals (red) were detected only in ciliated cells in human lung tissue. Left image: ciliated cell marker tubulin (green) localized with CA12 immunofluorescence (red). Right image: goblet cell marker MUC5AC (green) did not co-localize with CA12 (red). Scale bars = 20  $\mu\text{m}$ .

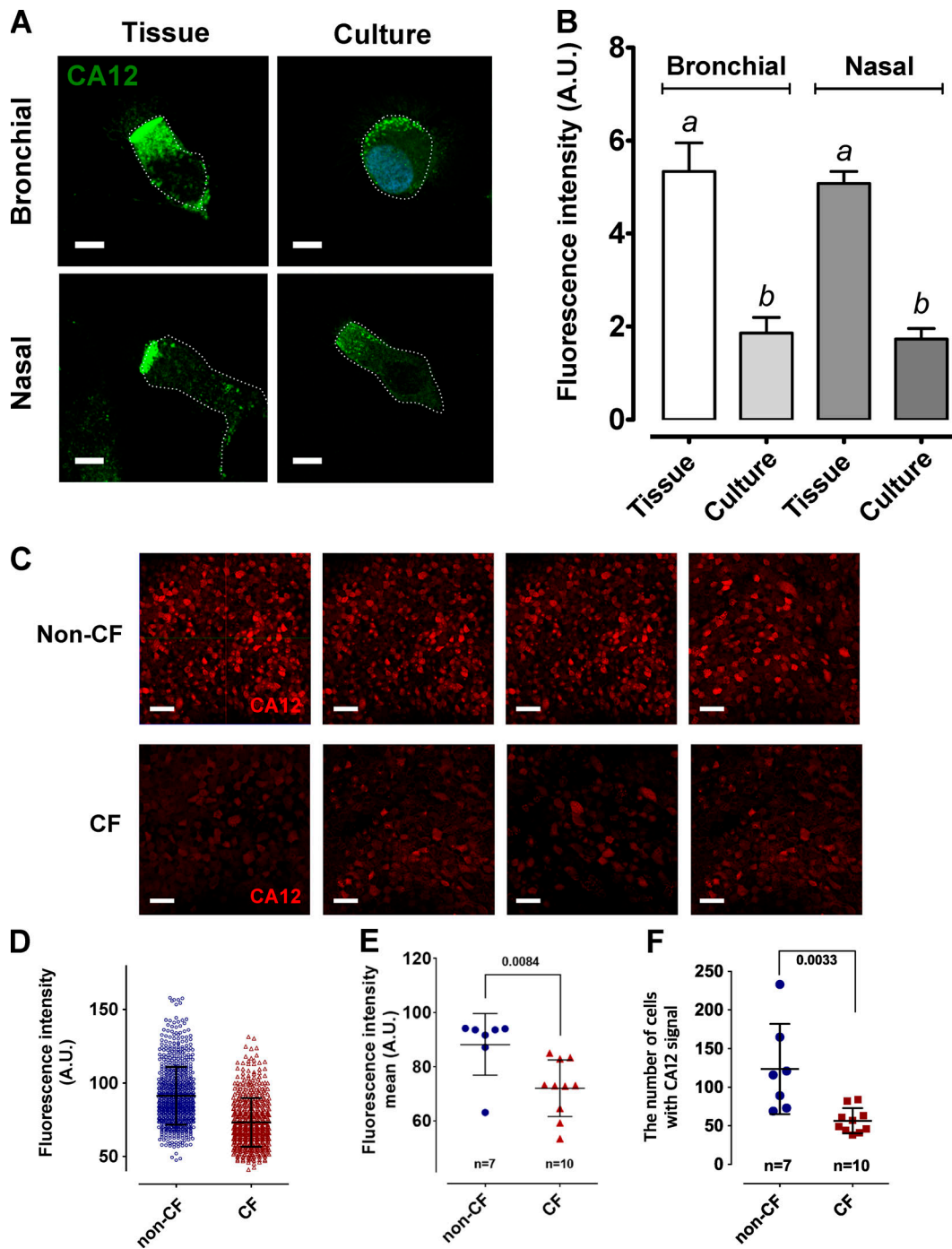


Figure S4. **CA12 immunostaining is reduced in CF bronchial and nasal cell cultures.** (A) Apical localization of CA12 in bronchial and nasal brushings (left images) and well-differentiated bronchial and nasal cells isolated from air-liquid interface cultures. White scale bars = 10  $\mu$ m. (B) Summary of CA12 immunofluorescence intensities measured as in A with identical microscope settings. Mean  $\pm$  SE, one-way ANOVA with Tukey's post-hoc test. *a* and *b* are significantly different; *n*/*P* value: 6–8/7.8  $\times$  10<sup>-6</sup>. (C) CA12 immunofluorescence in well-differentiated non-CF and CF HBEs (four images each condition). Fluorescence intensities were determined using the same settings and analyzed using IMARIS software. White scale bars = 20  $\mu$ m. (D) Summary of all single-cell CA12 immunofluorescence intensities from 8–10 different cultures (*n* = 751 non-CF cells and 568 CF cells). Error bars represent mean  $\pm$  SE. (E) Mean CA12 immunofluorescence intensities from individual cultures (each average of 50–100 cells was considered *n* = 1). Mean  $\pm$  SE, Student's *t* test; *P* = 0.0084. (F) Number of cells with CA12 immunofluorescence in cultures of cells from two non-CF and two CF patients. Mean  $\pm$  SE, Student's *t* test; *P* = 0.0033. A.U., arbitrary units.

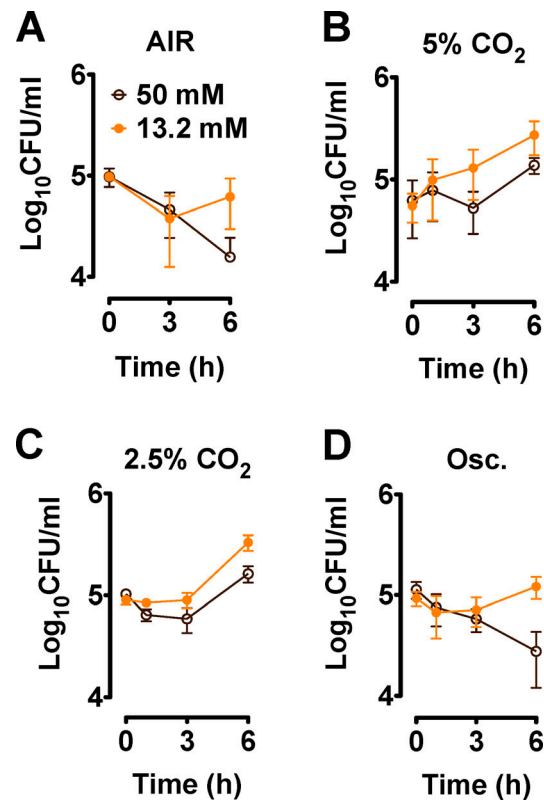


Figure S5. **HCO<sub>3</sub><sup>-</sup>-dependent killing is enhanced by PCO<sub>2</sub> oscillations in the presence of nutrients.** (A) Equilibration with room air (0.035% CO<sub>2</sub>) is bacteriostatic when artificial ASL (115 mM NaCl, 1.2 mM CaCl<sub>2</sub>, and 1.2 mM MgCl<sub>2</sub>) + 1% TBS is supplemented with 13.2 mM HCO<sub>3</sub><sup>-</sup> and bactericidal when it contains 50 mM HCO<sub>3</sub><sup>-</sup>. (B and C) Bacteria proliferate in nutrient-containing artificial ASL at both concentrations when exposed to constant 5% and 2.5% CO<sub>2</sub>, respectively. (D) Oscillations that yield the same mean PCO<sub>2</sub> (2.5%) as in C prevent bacterial growth and may be bacteriostatic (13.2 mM HCO<sub>3</sub><sup>-</sup>) or bactericidal (50 mM HCO<sub>3</sub><sup>-</sup>). The error bars represent mean ± SE.